Beyond the Local Volume: Surface Densities of Ultracool Dwarfs in Deep HST/WFC3 Parallel Fields

Christian Aganze,[1] Adam J. Burgasser,[1] Mathew Malkan,[2] Chih-Chun Hsu,[1]
Christopher A. Theissen,[1] Daniella C. Bardalez Gagliuffi,[3] Russel Ryan,[4] and
Benne Holwerda[5]

[1]*Department of Physics, University of California, San Diego, CA 92093, USA*

[2]*Department of Physics & Astronomy, University of California, Los Angeles, CA 90095, USA*

[3]*Department of Astrophysics, American Museum of Natural History, Central Park West at 79th Street, NY 10024,
USA*

[4]*Space Telescope Science Institute, 3700 San Martin Dr., Baltimore, MD 21218*

[5]*Department of Physics and Astronomy, 102 Natural Science Building, University of Louisville, Louisville KY 40292,
USA*

ABSTRACT

[will fill in this after all edits]

1. INTRODUCTION

The structure and evolution of the Milky Way is probed by specific and homogenous populations of stars. The Milky Way stellar density profile is smooth, fit to an exponential disk component and a power-law or flat spheroid for halo component (Jurić et al. 2008). Ultracool dwarfs (UCDs; M $\lesssim 0.1 M_\odot$, T_{eff} $\lesssim 3000$K; Kirkpatrick 2005) provide a new approach for studying the Galaxy as they are abundant in every environment throughout the Galaxy. UCDs are members of the late-M, L, T and Y spectral classes, and constitute $\sim 50\%$ of the total number of stars in the galaxy (Cruz et al. 2007, Chabrier & Baraffe 2000, Burrows et al. 2001, Bochanski et al. 2010). They have distinct spectra shaped by strong molecular absorption that are highly sensitive to their temperature, surface gravity and metallicity. In addition, these objects do not fuse hydrogen, hence, they cool down with time. This evolution of UCDs provides potential age diagnostics that have been exploited in stellar

cluster studies (Basri 1998; Luhman & Mamajek 2012; Martin et al. 2017) and searches of young moving groups near the Sun (Lopez-Santiago et al. 2006, Gagné et al. 2015, Mamajek 2015, Faherty et al. 2018).

UCDs are usually discovered in red optical and infrared sky surveys (DENIS: Delfosse, X. et al. 1999, 2MASS: Cruz et al. 2007; Kirkpatrick et al. 2010, WISE: Kirkpatrick et al. 2011; Cushing et al. 2011, UKIDSS: Marocco et al. 2015; Day-Jones et al. 2013; Burningham et al. 2013, CFBDS: Reyle et al. 2010, Gaia: Reylé 2018) but due to their intrinsic faintness, these samples are distance limited ($\leq$100pc). Hence, efforts to constrain the luminosity function have focussed on compiling volume-limited samples of UCDs within 20–25 pc of the sun (Cruz et al. 2007; Metchev et al. 2008; Reyle et al. 2010; Kirkpatrick et al. 2019; Bardalez Gagliuffi et al. 2019). However, UCDs cool with age; and older, metal-poor T-dwarfs populations are more dispersed into the galactic thick disk and halo (Burgasser et al. 2009; Zhang et al. 2019) hinting to a possible different formation mechanism, possible initial-mass function (IMF) variations (Bastian et al. 2010) or an interesting star-formation history (SFH). To further investigate these scenarios, it useful to conduct searches of UCDs populations beyond the local volume and further into the thick disk and halo of the Milky Way.

Deep pencil-beam imaging and spectroscopic surveys provide star-count data used to characterize stellar and UCD populations beyond the local volume. A common approach of selecting populations of UCDs, in the context of compiling a homogeneous sample of UCDs for follow-up studies in deep surveys, uses photometric selections anchored on a known sample of UCDs. Early work by Gould et al. (1997) sought to infer the dark matter content of the halo by measuring the halo luminosity function of the Hubble Space Telescope's Wide Field Camera 2 (HST-WFC2) and Planetary Camera (PC1) deep fields. They found 47 M dwarfs with $M_V >$13.5 consistent with a turning point in power law the mass function at M $\sim$0.6 $M_\odot$ from α=-1 to α=0.44. Subsequent studies by Kerins (1997); Chabrier & Mera (1997) concluded that the contribution of low-mass stars (M$\sim$0.3 $M_\odot$) to the halo luminosity function is less than 1%. Later work by Reylé & Robin (2001) compiled star-count data from different shallow and deep fields surveys and derived a scale height of 800 pc and a scale length

of 2500 pc, and a local density of 10^{-3} pc^{-3} for stellar masses of 0.2–0.8 $M_\odot$ consistent with a mass function $\frac{dN}{dM} = M^{-0.5}$.

In the context of using a sample of distant UCDs to probe galactic structure, Ryan Jr. et al. (2005) searched 15 deep parallel fields from the Hubble Space Telescope star-count data and estimated a scale of ∼350 pc for L & T dwarfs. Later work by Ryan et al. (2011) found 17 late M, L and T dwarfs in 231.90 arcmin^2 of WFC3 imaging of the GOODS fields using a combination of wide and narrow-band filter colors. They estimated a disk scale height of 290±39pc consistent with work by Pirzkal et al. (2005). In addition to poor estimate of spectral types, these samples were contaminated with various non-stellar sources that could not be identified in the absence of spectral information. To push towards a larger and pure sample, Holwerda et al. (2014) identified 274 in 227 arcmin^2 M-dwarfs (to a limiting magnitude F125W=25) from the HST-WFC3 Brightest of Re-ionizing Galaxies (BoRG, Pirzkal et al. 2009) survey, using an optical and near-infrared colors and determined their spectral types using V-J color-M-dwarf subtype relation (Pirzkal et al. 2009). They found a slightly higher density of M-dwarfs identified in the Northern fields compared to the Southern Fields, and a disk scale-height of 0.3–4kpc with a dependence on subtype. The overall M-dwarf scale height was ∼600 pc, a number that is much larger than previous estimates mostly due to large uncertainties in the fit. Van Vledder et al. (2016) reanalyzed these data using a Markov Chain Monte Carlo method to fit the statistic to a galactic model including a thin disk, thick disk, and halo component. They derived a scale height of 290^{+20}_{-19} pc and a central number density of $0.29^{+0.20}_{-0.13}$ pc^{-3}, with no correlation of model parameters with M-dwarf subtype, and consistent with previous studies. However, these studies do not probe statistics for later types. Recent work by Sorahana et al. (2018) found 3665 L dwarfs brighter than z=24 by searching 130 square degrees of the Hyper Suprime-Cam Subaru Strategic Program data and found an average L-dwarf scale height of 340–420 pc. Carnero Rosell et al. (2019) compiled a list of 11,745 photometrically classified L0-T9 dwarfs distances up to ∼ 400 pc by searching ∼2,400 deg^2 of the Dark Energy Survey (DES) data at a limiting magnitude of z=22. They estimated a large scale height of ∼ 450 pc. These last two studies provide another constraint on the number density of L dwarfs in the Galaxy using large samples (N>10^3); however, as

in many imaging surveys, poor accuracy in spectral types significantly affects the derived parameters. Ultimately, the large uncertainties on spectral types of UCDs in imaging surveys poorly constrain their distances, and deep spectroscopic follow-up of these sources is not a priority for precious HST time.

A parallel approach is to use pencil beam sample of spectra in red optical and near infrared (NIR) with no prior selection of source type. NIR spectroscopy, in particular, samples the peak of UCD spectral energy distribution and broad molecular features that guide UCD classification schemes (Kirkpatrick 2005, Burgasser et al. 2006). Pirzkal et al. (2005) identified 18 M and 2 L dwarfs in the Hubble Ultra Deep Field (HUDF) and estimated their spectral types by fitting templates from Kirkpatrick et al. (2000) to their Gradient-Assisted Photon Echo Spectroscopy (GRAPES) spectra in the optical wavelength regime. This study estimated a disk scale height of 400 ± 100 pc for M and L dwarfs. Another study by Pirzkal et al. (2009) used deep Advanced Camera for Surveys (ACS) slitless grism observations of the Probing Evolution And Reionization Spectroscopically (PEARS) fields (as part the Great Observatories Origins Deep Survey (GOODS) fields, Giavalisco et al. 2004) down to a z=25 and spectroscopically identified 43 M4-M9 dwarfs. Using a thick and thin disk model, the study estimated a scale height for the thin disk of $\sim$370 pc, and $\sim$100 pc for the thick disk, a halo fraction between 0.00025–0.0005 consistent with previous estimates.

Masters et al. 2012 discovered 3 late T dwarfs the WFC3 infrared Spectroscopic Survey (WISPS) fields (Atek et al. 2010) identified by their strong CH_4 and H_2O absorption features. The sample size was not large enough to put meaningful constraints on the scale height or the luminosity function L and T dwarfs beyond the local volume. In this paper, we expand upon this study by developing an effective method to select UCDs in similar surveys.

Section 2 describes the data, section 3 describes the selection process, section 4 discusses the result compared to a Monte-Carlo simulation

2. DATA

2.1. *Survey Data*

We obtained data from two pure-parallel surveys: the WFC3 Infrared Spectroscopic Parallel Survey (WISPS, Atek et al. 2010) and 3D-HST (Momcheva et al. 2016, Brammer et al. 2012, Skelton et al. 2014). These two surveys used the IR channel of the WFC3 camera (Kimble et al. 2008) providing low-resolution G102 ($\lambda = 0.8$–1.17 μm, R$\sim$210) and G141 ($\lambda = 1.11$–1.67 μm, R $\sim$130) grism spectra. Removal of the slit mask allows for the overlapping spectra of the 136×123 arcsec inner FOV of the WFC3 camera. The WISP survey is a 1000-orbit HST parallel survey covering 390 fields ($\sim$1500 arcmin^2) that follows observing programs accepted on the Cosmic Origins Spectrograph (COS) and Space Telescope Imaging Spectrograph (STIS). 3D-HST is also a parallel survey of 248-orbits spanning $\sim$600 arcmin^2 as part of Hubble Cycles 18 & 19. This survey targets four extra-galactic fields: The All-wavelength Extended Groth Strip International Survey (AEGIS, Davis et al. 2007), Cosmic Evolution Survey (COSMOS, Scoville et al. 2007), Ultra-Deep Survey(UKIDSS-UDS, Lawrence & Others 2007), the Great Observatories Origins Deep Survey (GOODS-South and GOODS-North, Giavalisco et al. 2004), using the ACS/G800L and WFC3/G141 grisms in parallel. Figure **??** shows an WCF3 exposure of one of fields in WISP.

Both surveys provide photometry information from various surveys and instruments in narrow-band and broad-band filters; we used photometric data acquired using F110W, F140W, F160W filters. Figure 7 displays these filter profiles to other standard filters. We report a detailed list observations for all the fields in Table 6 as well as a sky map of all the pointings.

2.2. *Data Reduction*

Data reduction for the WISP survey is performed using the `AXe` software Cookbook (Kuntschner et al. 2013; Kümmel et al. 2009) and a custom pipeline described by Atek et al. (2010); we did not perform any further reduction the both the spectroscopic data or the images provided by the survey. The data 3D-HST Survey deviates from the pipeline `AXe` pipeline and implements a full custom reduction pipeline. We used data products described by Momcheva et al. (2016) and the photometric catalog of sources in Skelton et al. (2014) retrieved from https://3dhst.research.yale.edu/Home.html

3. SELECTION OF UCDS

3.1. *F-test and SNR cuts*

The 3D-HST survey is designed to measure accurate redshifts from emission lines, hence the spectra obtained from the data not continuum-corrected as shown in Figure 7. We obtained a correct continuum of each 3D-SHT spectrum by dividing the flux of the spectrum and the sensitivity curve of the detector provided in the data. In addition, we fitted each spectrum to UCDs SpeX spectra of spectral standards using χ^2 minimization following the method of Kirkpatrick et al. (2010) to obtain a preliminary spectral type classification all available WISP and 3D-HST spectra. We also compared every spectrum to a straight line in the same wavelength region and measured χ^2. The χ^2 of a line (l) or a standard (std) is given by

$$\chi^2(\text{l}, \text{std}) = \sum_{\lambda=1.15\mu\text{m}}^{1.65\mu\text{m}} \frac{(R(\lambda) - \text{Sp}(\lambda))^2}{\sigma_{sp}^2} \tag{1}$$

where $R(\lambda)$ is the reference spectrum (spectral standard or line), $\text{Sp}(\lambda)$ is a WISP or 3D-HST spectrum and σ_{sp}^2 is the noise in the WISP or 3D-HST spectrum. We use an F-fest as a statistical test to separate noisy/flat spectra from the rest of the sample implemented by `Scipy` Jones et al. 2001– as `scipy.stat.f`. A flat spectrum is defined as having $F(\chi_s^2/\chi_l^2) > 0.5$. An illustration of a various types of spectra and their statistics is provided in figure x. We also defined a signal-to-noise ratio in the J-band continuum (SNR-J) in the wavelength region of 1.2 μm $\leq \lambda \leq$ 1.3 μm for all the spectra in both surveys. Point sources are identified both catalogs using flags: `STAR_FLAG` = 1 in 3D-HST and `CLASS_STAR` $\neq$ 0 in WISP. In summary, we obtained 270436 grism spectra in both surveys that have corresponding photometry in any of the three bands (F110W, F140W, F160W), among these, 194437 spectra are from WISP and 75999 are from 3D-HST. As a cut, we selected 27737 objects in both surveys that are flagged as point sources and have a SNR-J $>$3. Finally, only 637 point sources with SNR-J $>$3 satisfy and F-test criterion $>$0.5. We then used the methods described in 3.4 to define UCDs candidates to be confirmed by visual inspection.

3.2. *Spectral Indices*

3.2.1. *Definition*

UCDs display strong CH_4 and H_2O molecular features in 1.1 μm $<\lambda<$1.7 μm region (Burgasser 2001), they can be separated from other stellar/galaxy populations using these features. Spectral Indices have traditionally been used to determine spectral types (Tokunaga & Kobayashi 1999, Cushing et al. 2000, Allers et al. 2007, Burgasser et al. 2007). Thus, we defined spectral indices in five wavelength bands: 1.15–1.20 μm, 1.246–1.295 μm, 1.38–1.43 μm, 1.56–1.61 μm, or 1.62–1.67 μm; denoted by H_2O-1, J-Cont, H_2O-1, H-Cont, and CH_4 respectively. Each index is the ratio of the median flux in these bands given by

$$Index = \frac{\langle F(\lambda_1 < \lambda < \lambda_2)\rangle}{\langle F(\lambda_1 < \lambda < \lambda_2)\rangle} \tag{2}$$

tracing the H_2O and CH_4 features as well as the J and H band continuum. We measured uncertainties in each index by random sampling, assuming these uncertainties are Gaussian-distributed.

3.3. *Calibration Samples*

We trained these spectral indices a on well-characterized sample of similarly-typed template UCDs. These are 1525 M7-T9 low-resolution ($\sim$75-120), NIR (0.9-2.5 μm) spectra of nearby UCD templates from the SpeX Prism Library (SPL,Burgasser 2014a) with SNR >60. In addition, we use the 69 L0-Y1 UCDs from Manjavacas et al. (2018) observed with WFC-3, and 22 Y dwarfs obtained by Schneider et al. (2015) that we will refer to as the Manjavacas and Schneider datasets. We measured these indices for all these data sets, we observe an expected trend in spectral indices for similar subtypes with the changing strength of H_2O and CH_4 features in the spectrum. We use these three data sets as a training set to to design selection criteria for UCDs candidates in WISP and 3D-HST.

3.4. *Box Selection Criteria*

We define selection criteria using boxes/parallelograms in each of 45 independent, 2D spectral index-spectral index spaces. Ideally, UCDs with similar spectral types will cluster within the same region in these spaces, away from the contaminants while the evolution of H_2O and CH_4 bands with subtype should distinguish classes. To define the extent of each box, we fitted a central line to each of the M5–L0, L0–L5, L5–T0, T0–T5, T5–T9, subdwarfs, Y dwarfs subtype groups using

linear regression by minimizing χ^2. The equation that minimizes χ^2 for a simple linear fit is given

The values are $x_1 \ldots x_N$ and $y_1 \ldots y_N$ are the indices on the x and y-axes, and $\sigma_{y1}^2 \ldots \sigma_{yN}^2$ are the uncertainties in the y-axis spectral indices assuming Gaussian uncertainties. The choice of x-axis or y-axis are arbitrary since we do not prescribe which index is on the x-axis or y-axis but we choose all possible combinations of indices with no repetitions. The width of the box is determined by $x_{\min,\max} = \mathrm{median}_x \pm 3.0 \times \sigma_x$, where σ_x is the standard deviation in the x-values, while the vertices of each box are defined as by $(x_{\max}, y_{\max} = mx_{\max} + b \pm s)$ and $(x_{\min}, y_{\min} = mx_{\min} + b \pm s)$ where s is a scatter coefficient between the line and the indices also defined as

$$s = 3 \times \sqrt{1/N \sum_{i=1}^{N}(y_i - (mx_i + b))^2} \tag{3}$$

This method provides a simple and automatic prescription for selecting objects within a subtytpe given 3 parameters b, m and s; we assess the effectiveness of this method by defining a completeness and contamination statistic for each of the subtype group as follows:

$$CP = \frac{TEMP_s}{TEMP_{tot}} \tag{4}$$

$$CT = \frac{WFC3_s}{WFC3_{true}} - 1 \tag{5}$$

where $TEMP_s$ is the number of templates selected by the box, $TEMP_{tot}$ is the total number of SpeX templates, $WFC3_s$ is the number of WISPS and/or 3D-HST spectra selected by the box, $WFC3_{true}$ is the number of previously known UCDs in WISPS and /or 3D-HST after visual confirmation. We only employed criteria with the lowest contamination and highest completeness to select UCDs, and all the index selection boxes are >85 % complete. We report b, m, and s for all the indices with the lowest contamination in table 1 We used this selection process iteratively i.e., we first applied the best box for each subtype, that is the box with lowest contamination and highest completeness, we visually inspected the selected spectra, updating $WFC3_{true}$ through this step. We then recomputed CT and CP for all the boxes and repeat this process until there were no new candidates. As a final step, after all selection has been applied, we visually inspected at all the x candidates to find any

objects missed by spectral indices, we further discuss the effects of our selection process in section **??**. The best criteria for each of the subtype groupings are summarized in table x.

3.5. *Spectral Classification and Visual Inspection*

After visual inspection of the all the candidates and removal of remaining contaminants, we compiled a sample of UCDs with accurate spectral types. To determine the spectral type classification of each UCD, we compared each of WISP& 3D-HST UCD to SpeX spectral standards using the lowest χ^2 statistic following the procedure of Kirkpatrick et al. (2010).

In addition to spectral types, we computed photometric distances for all the UCDs using absolute 2MASS J and H relations from Dupuy & Liu (2012). Given that these relations are defined for J and H filters, we inferred similar relations for F110W, F140W, F160W filters using the following steps: we first computed an offset between 2MASS J and H magnitudes and AB Hubble magnitudes [1] by convolving the a SpeX standard for that spectral type with the respective filter. This offset in convolutions is then added to the absolute magnitude-spectral type relations in 2MASS J, H filters to obtain the new relation in Hubble filters. We used these relations throughout this study to determine distances given an apparent F110W, F140W or F160W magnitude and a spectral type.

3.6. *Random Forest Classifier*

As an alternative to making an arbitrary cutoff using an F-test, we trained a random forest classifier by deploying `RandomForestClassifier` implementation by `scikit-learn` (Pedregosa et al. 2012) to classify potential UCDs in both surveys. Random forests have been shown to reliably predict M-dwarf subytpes based on colors (Hardegree-Ullman et al. 2019), and in principle, our index selection criteria act as proxy for colors. The training set is composed of spectral templates defined in 3.3 and a list of 20 WISPS & 3D-HST UCDs visually confirmed and selected by F-test cutoff and the method described in 3.4. The total number of objects in the training set is 3610, made of 1856 visually confirmed non-UCDs, 1525 SpeX templates, 77 objects from the Manjavacas set, and 22 objects

---

[1] 3D-HST F140W and F160W magnitudes are computed using reported fluxes in photometric catalogs in Skelton et al. 2014 as -2.5 $log_{10}F + 25$, while WISPS magnitudes are used as reported

from the Schneider set and 20 UCDs from WISPS & 3D-HST. We used a set of 15 features including all 10 spectral indices as proxy for color, the signal-to-noise ratio in the J-continuum (SNR-J), the two χ^2s and their ratio, and the F-test value. We used two labels: UCD, and non-UCD to describe ultracool dwarfs and the rest of the set. We split the training set and the test set as 50% and 50% and scaled all features between in the range [0, 1] using `MinMaxScaler`. We achieved an accuracy score of 94.8% in cross-validation. We show the confusion matrix in figure 10

In summary, we have presented two methods for selecting UCDs in deep HST surveys potentially applicable future infrared parallel surveys. Both methods rely on spectral indices defined to trace H_2O and CH_4 features prominent in the NIR band of UCDS. The box selection method is efficient (completeness >80%) but with relatively high contamination rates that could be significantly reduced by eliminating the lowest SNR sources. This method is not effective for selecting very low SNR sources due to large uncertainties in spectral indices (SNR-J<3.0) and early M-dwarfs as the absorption features in these wavelength ranges are shallow. However, these spectral indices are designed to selected T-dwarfs with high accuracy (completeness >90%, contamination <1%). The overall contamination rate of this method is $\sim 19\%$. A second method uses a random forest classifier to distinguish UCDs from other extragalactic contaminants or artifacts with an accuracy score of 94.8% in cross-validation. The overall contamination rate of this method is $\sim 67\%$. Both methods rely on a training set of known UCD samples and can be combined. 17 out of the total of 27 UCDs were found by both the box selection method and the classifier.

4. RESULTS

4.1. *M, L, T Dwarfs Candidates*

We found 25 L and T dwarfs. We purposely excluded M-dwarfs in the sample given that H_2O and CH_4 features in these regions are weak. We report their distances and photometry in table 2. We found L-dwarfs up to $\sim$1000pc, and T-dwarfs up to $\sim$500 pc; the distribution of distances for all the UCDs is shown in Figure **??** and we recovered the 3T-dwarfs discovered by Masters et al. 2012.We found 14 L dwarfs in both surveys, 11 T dwarfs in WISP and 3 L dwarfs in HST-3D, all

with a SNR-J >4. The closet L dwarf in the sample is WISP 0927+6027, with spectral type of L0 at ∼320±10pc and a SNR-J of ∼320, while the farthest L-dwarf is WISP 1154+193 with spectral type of L3 at a distance of ∼1800±650 pc. We also found 9 T dwarfs, 7 in WISP and 2 in 3D-HST. WISPS T dwarfs include T7 WISP 1232-0033, T9 WISP 1305-2538 and T4 WISP 0307-7243 found by Masters et al. 2012, and are the latest T dwarfs in the sample. The farthest T dwarf in the sample is UDS 0217-0514 at a distance of 2400±360pc and with a SNR-J of ∼9, the closet T dwarf in the sample is WISP 1232-0033 at a distance of 2400±360pc and with a SNR-J of 9. AEGIS1418+5242 is the second T dwarf in 3D-HST with a spectral type of T4 and at a distance of 540±80pc at with a SNR-J of 24.

4.2. *Comparison to Predictions*
4.2.1. *Magnitude Completeness*

We aim to constrain the number density of UCDs; an accurate estimate of the effective distance/volume of each pointing is crucial. Momcheva et al. 2016 reported the effective depths of all the pointings in 3D-HST, however, given the SNR cut, we expect the a brighter limit than these reported depths. Hence, we adopted the faintness limits of F110W=22.0, F140W=21.5, F160W=21.5 for WISP fields, and F140W=22.5, F160W=22.5 for 3D-HST fields. For the bright end, we used the bright limits of F110W=18.0, F140W=16.0, F160W=16.0 for WISPS fields and F140W=16.0, F160W=16.0 for 3D-HST fields following the peak of the distribution of magnitudes (Figure **??**) for all the point sources satisfying the SNR cut. These bright limits correspond to limiting distances hence effective volumes for each spectral type, using the absolute magnitude spectral type relation from Dupuy & Liu 2012

4.2.2. *Selection Function*

Because we applied several selection criteria to narrow down our sample for visual confirmation, it is possible we may have missed a few UCDs in the WISPS/3D-HST fields; particularly low SNR or peculiar objects due, in part, to uncertainties in spectral indices. To fully quantify these effects, we generated a distribution of spectra uniformly sampling our SNR distribution across a wide range

of SNRs and measured their recovery rate through this selection process. To simulate a sample for spectra with various SNR-Js, we degraded a sample of chosen spectra from the SpeX sample by selecting at least 20 highest SNR objects in the SpeX sample per spectral type, and added Gaussian noise to these spectra until the overall SNR to noise in the spectrum is reduced below 3.0. We computed all relevant statistics for each of these generated spectra, including SNR-J, spectral indices, F-test, and the two χ^2s. We applied our selection processes to this sample of simulated spectra by measuring spectral indices and applying first f-test criterion where F-test >0.5, box index-index selection criteria and the random forest classifier. The fraction of spectra selected per spectral type per SNR bin is defined as the probability of selection of an object within Δ SNR-J bin of 2.0. We denote this probability of selection of $\mathcal{S}(\text{SNR-J, SpT})$

$$\mathcal{S}(\text{SNR-J, SpT}) = \frac{N_s}{N_{tot}}$$

where N_s is the number selected spectral type and SNR bin, and N_{tot} is the total number of objects in that bin.

4.2.3. *Number Densities, Monte-Carlo Simulation*

To compute the expected number of UCDs in each spectral type bin, we simulated a semi-empirical luminosity function, which we multiply by the effective volume of each spectral type corrected by our selection function. We followed these steps:

- We first simulated a sample of 10^5 objects in a power law mass function for a range of masses 0.02 M$_\odot$and 0.15 M$_\odot$as

$$\frac{dN}{dM} = \left(\frac{M}{M_\odot}\right)^{-0.6} \tag{6}$$

  normalized to 0.0055 pc^{-3} at M=0.10 M$_\odot$ (Reid et al. 1999, Chabrier 2001)

- We assigned each of these UCDs an age drawn from different star-formation histories: a uniform age distribution spanning 100 Myr–10 Gyr, a range of age exponential age distributions ($\beta \in$ [0.1, 10.0]) given by

$$P(t) \sim e^{\beta t} \tag{7}$$

and two predefined distributions from Aumer & Binney (2009) and cosmic age distribution from Rujopakarn et al. (2010)

- We assigned a temperature using UCD evolutionary models from Baraffe et al. (2003) converted to a spectral types using the relation from Filippazzo et al. (2015). We defined $\Phi(SpT)$ as this normalized distribution of spectral types.

- To account for the effects of galactic structure,we computed an effective volume for each spectral type defined following Burgasser (2007) defined as

$$V_{eff}(SpT) = \frac{1}{3}(d_{max}^3 - d_{min}^3) \times \Delta\Omega \times V_c \tag{8}$$

. Where $\Delta\Omega$ is the solid angle of the pointing and $d_{max,min}$ are the effective maximum or minimum distances given by

$$\log d_{min,max} = \frac{1}{5}(m - M(SpT)) + 1 \tag{9}$$

.V_c is a volume correction term, to account for the galactic structure obtained by integrating the galactic density as

$$V_c(l,b) = \frac{\int_0^{\delta x} \rho(x,l,b))x^2 dx}{\int_0^{\delta x} \rho_0 x^2 dx} \tag{10}$$

where x is the 3D- galacto-centric distance in along the line of sight of the field, and $\rho(x)$ is the galactic density along that line of sight. We set $\delta x = d_{max} - d_{min}$ as the total depth of a given pointing. We assumed a standard galactic structure model similar from Jurić et al. (2008)

- The spatial density of stars in each pointing is given by

$$\rho(R,z) = \rho_{thin} + \rho_{thick} + \rho_{halo} \tag{11}$$

$$\rho_{thin} = \rho_0 \exp\left(-\frac{|z - Z_\odot|}{H_{thin}}\right) \times \exp\left(-\frac{R - R_\odot}{L_{thin}}\right) \tag{12}$$

$$\rho_{thick} = \rho_0 \times f_{thick} \times \exp\left(-\frac{|z - Z_\odot|}{H_{thick}}\right) \times \exp\left(-\frac{R - R_\odot}{L_{thick}}\right) \tag{13}$$

$$\rho_{halo} = \rho_0 \times f_{halo}\left(\frac{R_\odot}{\sqrt{R^2 + (z^2/q^2)}}\right)^{-p} \tag{14}$$

H_{thin}, H_{thick} are the scale height of the thin and thick disk, L_{thin}, L_{thick} are the scale length of the thin/thick disk, q is the axial ratio the halo sphere, p is the flattening parameter and f_{thick}, f_{halo} are the fraction of stars in the thin thick disk and the halo.

- Given that our selection function is a function of both SNR-J and spectral type, we must assign a SNR-J to the distribution of 10,000 simulated objects. We computed a distribution of distances where the probability is given by

$$P(d_{min} < d < 2 \times d_{max}, l, b) \sim d^3 \times V_c(l, b) \tag{15}$$

where l, b are galactic latitude and longitude. After assigning each simulated UCD a distance, we computed an apparent magnitude using a polynomial to fit log SNR-J to the absolute apparent magnitudes of the WFC3 UCD sample (Figure x).

- We then used our most selective selection function $\mathcal{S}$ to assign a probability of selection/detection to each of the of the simulated objects.

- The expected number of sources per spectral type is given

$$N_{exp}(\text{SpT}) = \rho_0 \times V_{eff}(SpT) \times \sum_i \mathcal{S}_i n_i(SpT) \tag{16}$$

. Where n_i is the number of objects in a spectral type bin and S_i is the probability of selection for each object in that spectral type bin. We compared these numbers to the observed numbers of UCDs for each age distribution in figure 19

5. SUMMARY & DISCUSSION

The measured number of T-dwarfs is consistent with expectations given atmospheric cooling effects (Burgasser 2004) from evolutionary models. As UCDs age, they quickly pile up on at the lower end of the spectral type distribution and cooler temperatures. Ryan et al. (2017) estimated a change in scale height of (ΔH $\sim$50 pc) in the mid-L dwarf regime by comparing galactic models for different cooling scenarios; while the scale height in for M-dwarf remains constant independent of subtype. Despite the high accuracy in spectral types for the sample of UCDs presented in this study, the small sample of size of 20 could not accurately constrain the scale height for each spectral type.

Moreover, the L/T transition region is sensitive to unresolved binaries (Bardalez Gagliuffi et al. 2014). Burgasser (2007) shows that given a spectral binary fraction of $\sim 10 \%$, the surface densities for volume-limited sample of primaries and combined systems are similar but present a slight bump ($\Delta\Sigma \lesssim 5\times 10^{-5}$ deg^{-2}) for early T dwarfs. Given our total search area of ~ 0.6 deg^2, we do not expect a significant effect of the spectral binary fraction to the reported densities, hence we assumed that none of the UCDs in this study are unresolved binaries in our simulation.

Metallicity effects affect the number of subdwarfs we expected in this sample. UCDs in the thick disk and the halo have similar kinematic ages with stellar populations in these parts of the Galaxy; and UCDs at different metallicities follow different evolutionary tracks. L subdwarfs in the local neighborhood are therefore rare, and this study does not significantly probe large volumes in the thick disk and halo. Lodieu et al. (2017) found $0.04\times$ deg^{-2} L subdwarfs in the UKIDSS/SDSS fields; in fact, we expect the number of subdwarfs to be ~ 400 times lower than the expected number of dwarfs in the sample. Although the parallel fields in 3D-HST & WISP are deep, the total search area remains low, hence it is not surprising that we did not find any L subdwarfs in the sample.

Future space missions such as JSWT, Euclid will be contaminated by UCDs. Ryan Jr. & Reid (2016) predicted that the number density of UCDs (M8–T8) in JSWT fields peaks around J$\sim$24 mag with a total surface density of $\Sigma \sim 0.3$ arcmin^{-2}. With the *Large-Scale Synopitc Telescope* (LSST), and the *Wide-Field Infrared Survey Telescope* (WFIRST), we expect in increase in both sample size and spectral type accuracy, expanding the parameter space necessary to put significant constraint on

the star formation history of the MIlky Way in general and the mass function of UCDs in particular (LSST Science Collaboration et al. 2009, Spergel et al. 2015).
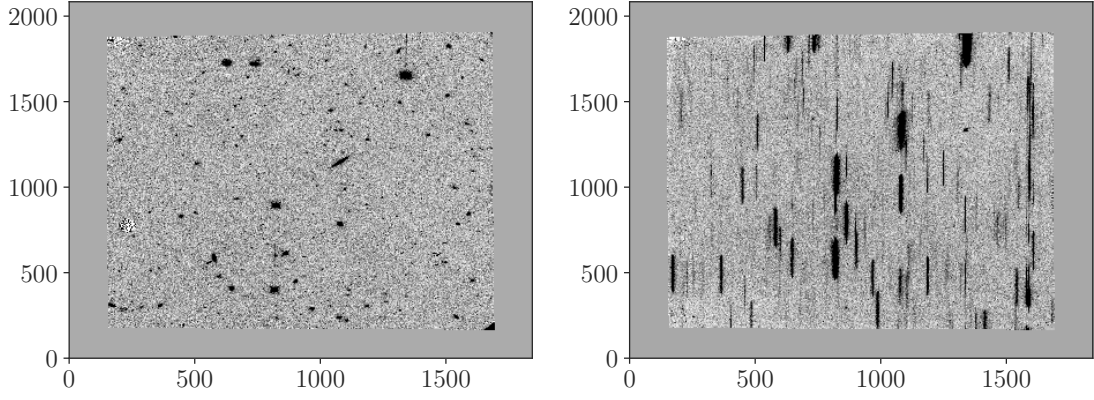
Figure 1. Example of a reduced grism spectrum of WISPS-01
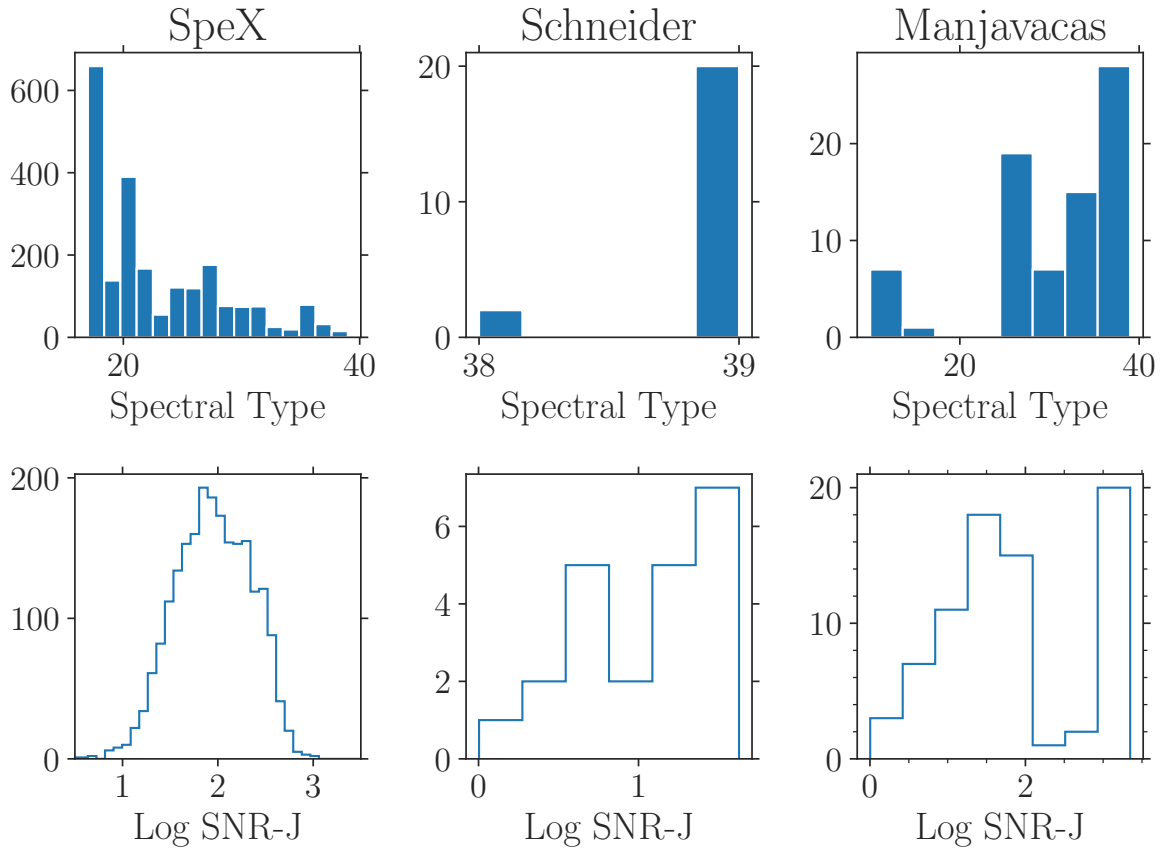
Figure 2. Calibration Samples of UCDs used in this study
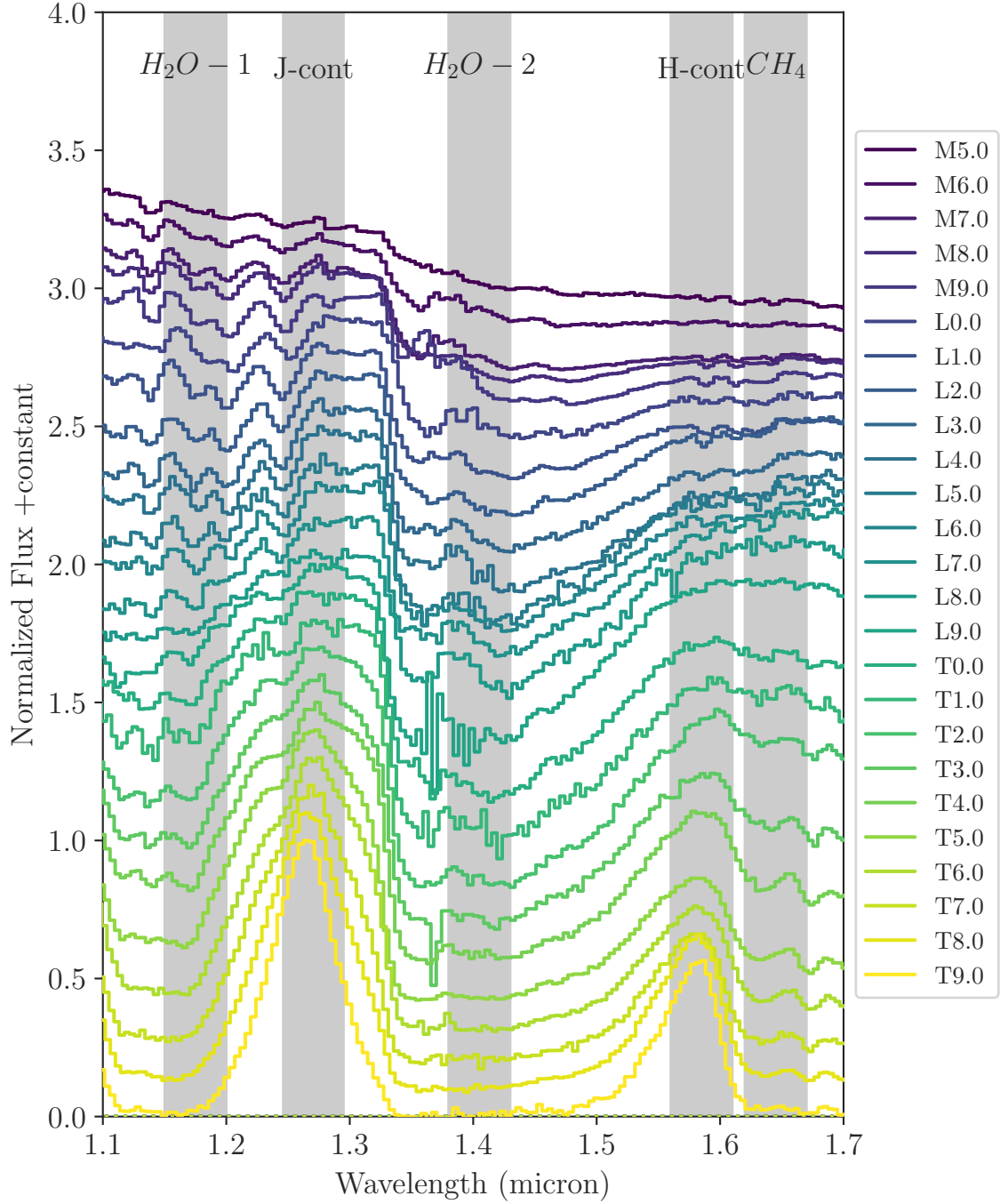
Figure 3. M5-T9 low resolution SpeX spectral standards (Kirkpatrick et al. 2010) with highlighted bands showing the definition of spectral indices used in this study
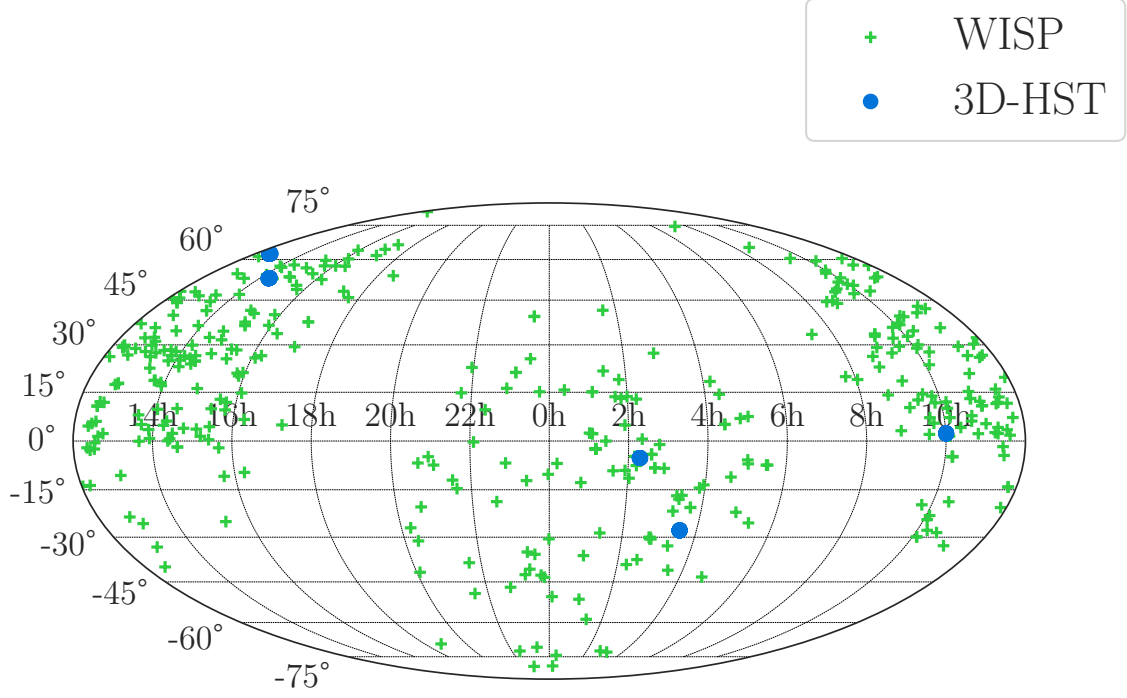
Figure 4. Sky map of all the pointings in WISPS and 3D-HST

Table 1. Best Selection Criteria

SpT Range	X-axis	Y-axis	m	b	s	Completeness	Contamination
L0–L5	H-cont$_/H_2$O -1	CH$_4$ $_/J-cont$	0.0	1.0	0.6	0.99	0.14
L5–T0	H-cont$_/H_2$O -1	H$_2$O -2$_/J-cont$	0.17	0.29	0.39,	0.95	0.165
T0–T5	CH$_4$ $_/H_2$O -1	H$_2$O -2$_/J-cont$	-0.1	0.28	0.43	0.93	0.135
Y dwarfs	H$_2$O -2$_/J-cont$	CH$_4$ $_/H-cont$	1.21	0.09	0.19	0.89	0.003
T5–T9	H$_2$O -1$_/J-cont$	CH$_4$ $_/H-cont$	1.61	0.03	0.09	0.95	0.003
Subdwarfs	H-cont$_/J-cont$	CH$_4$ $_/J-cont$	1.05	-0.01	0.04	0.9	0.031
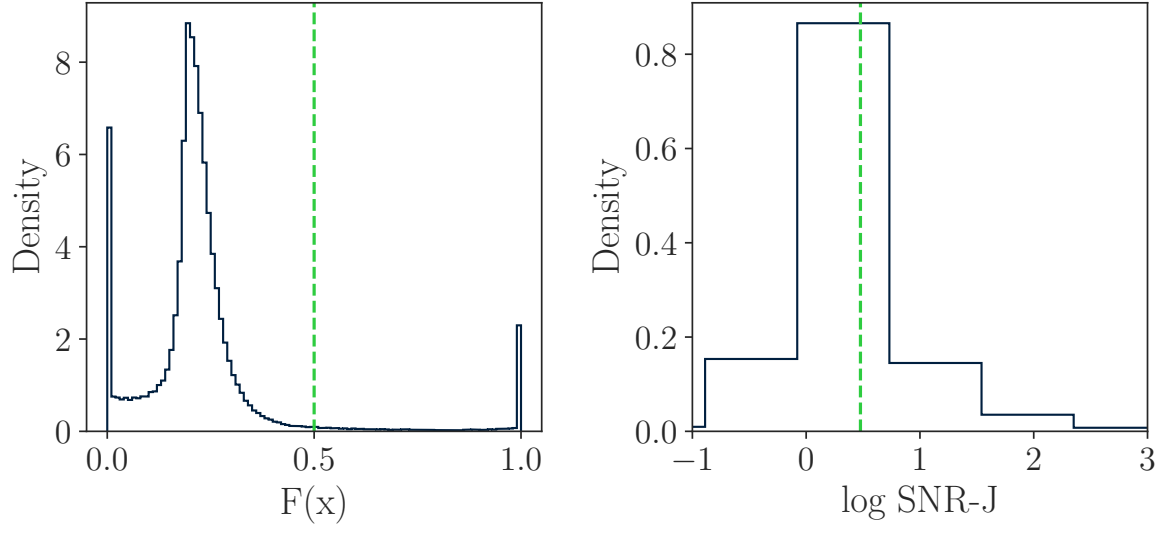
Figure 5. f-test and SNR-J distributions of all Spectra in both surveys
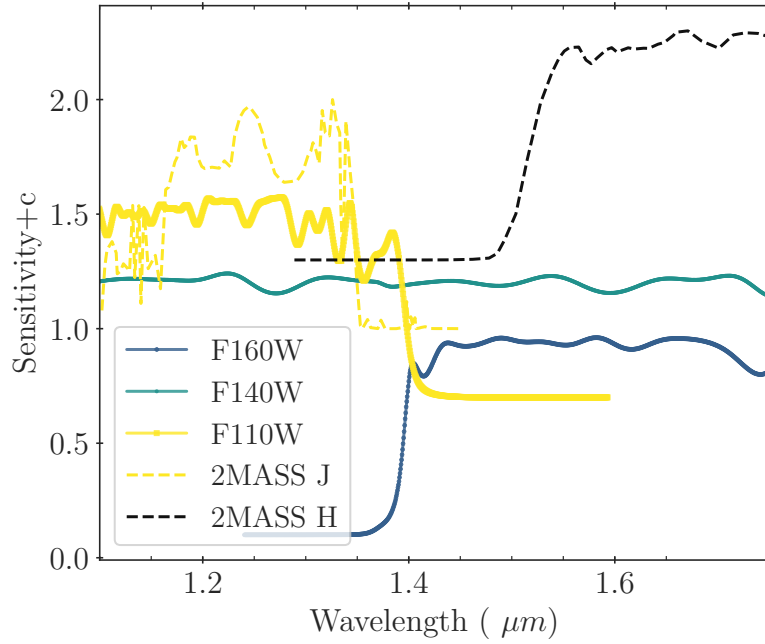
Figure 6. Comparison between different HST and 2MASS filters used in this study
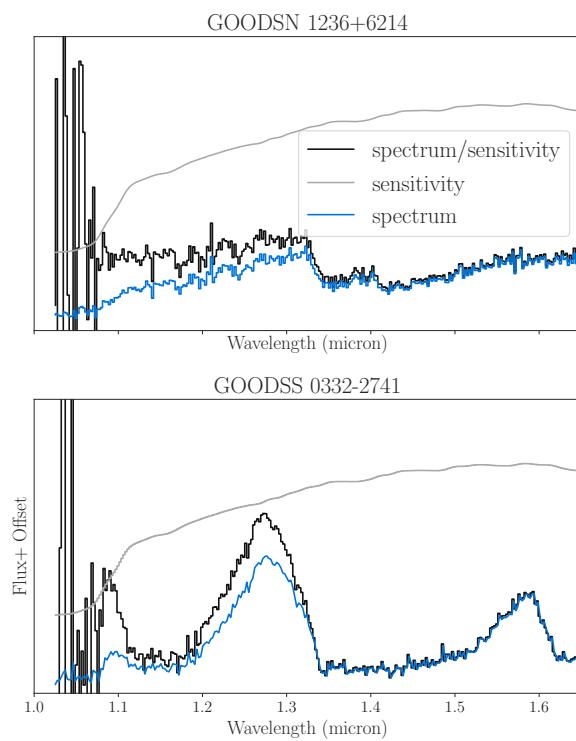
Figure 7. Example of 2 HST-3D spectra before and after continuum correction to obtain the correct slope. The sensitivity curve is plotted in grey.
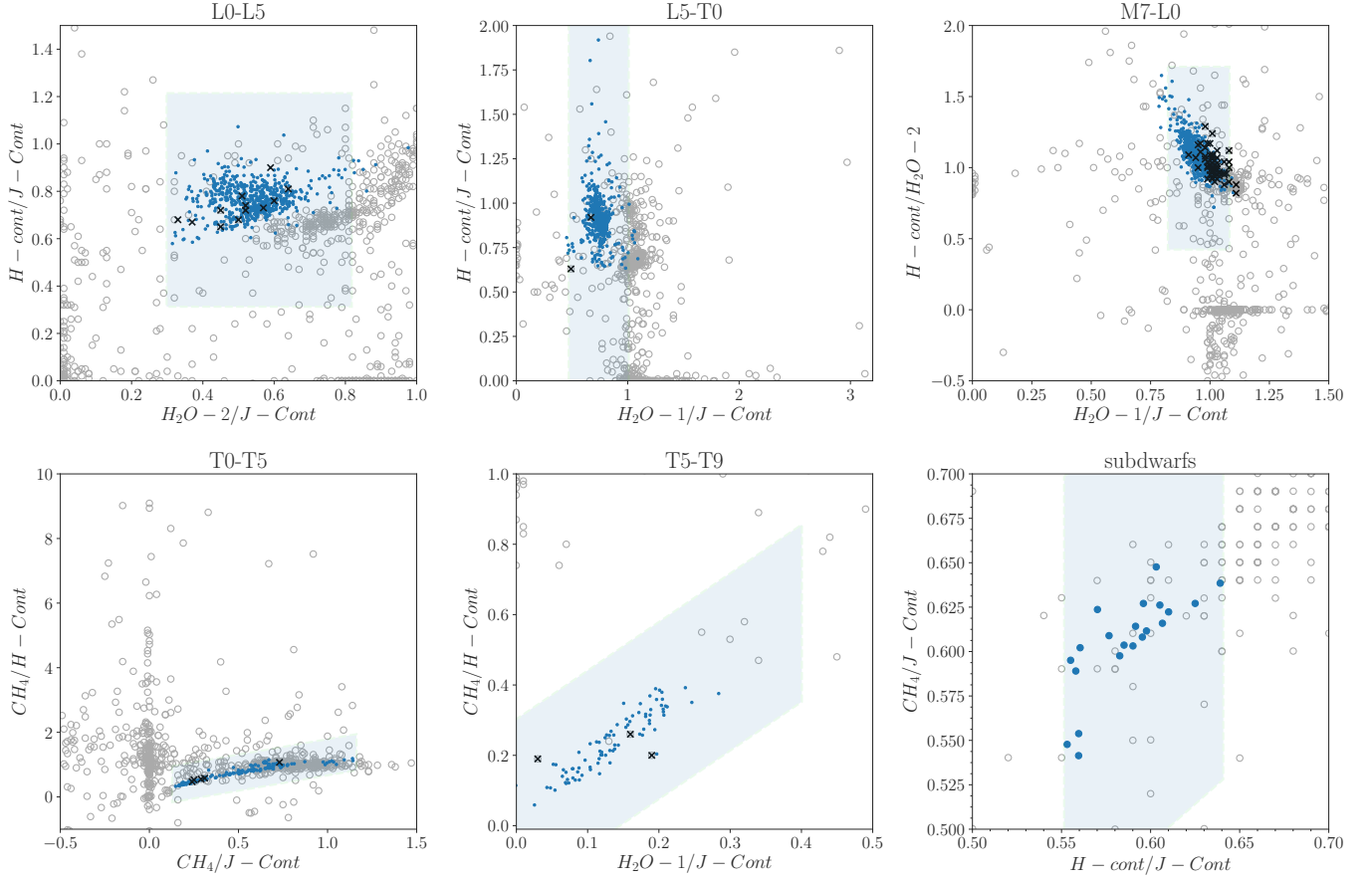
Figure 8. Best selection criteria for different subtype ranges. Both the calibration samples and the contaminants are shown
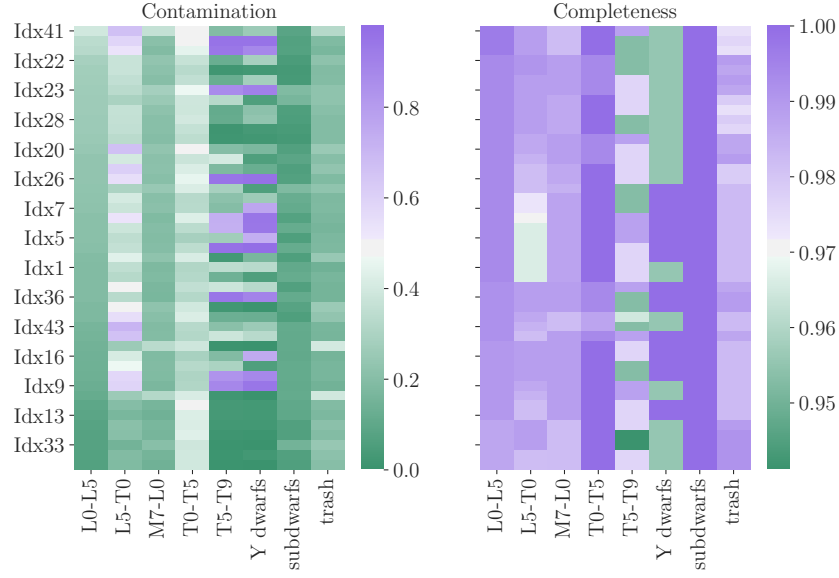
Figure 9. Visual Representation of CPT and COMP statistics for all possible combination of spectral indices for each subtype range. Although the overall completenesses of each box is high (>80%), the contamination may vary. We only use selection criteria with the lowest possible contamination, however, any comibination of these indices could be useful for selecting UCDS in other surveys
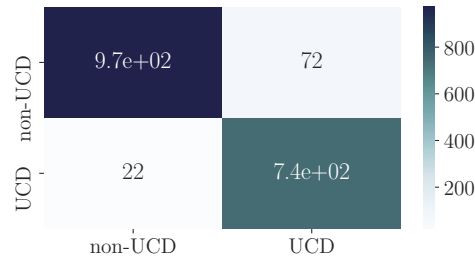
Figure 10. Confusion matrix for the random forest classifier used in this survey
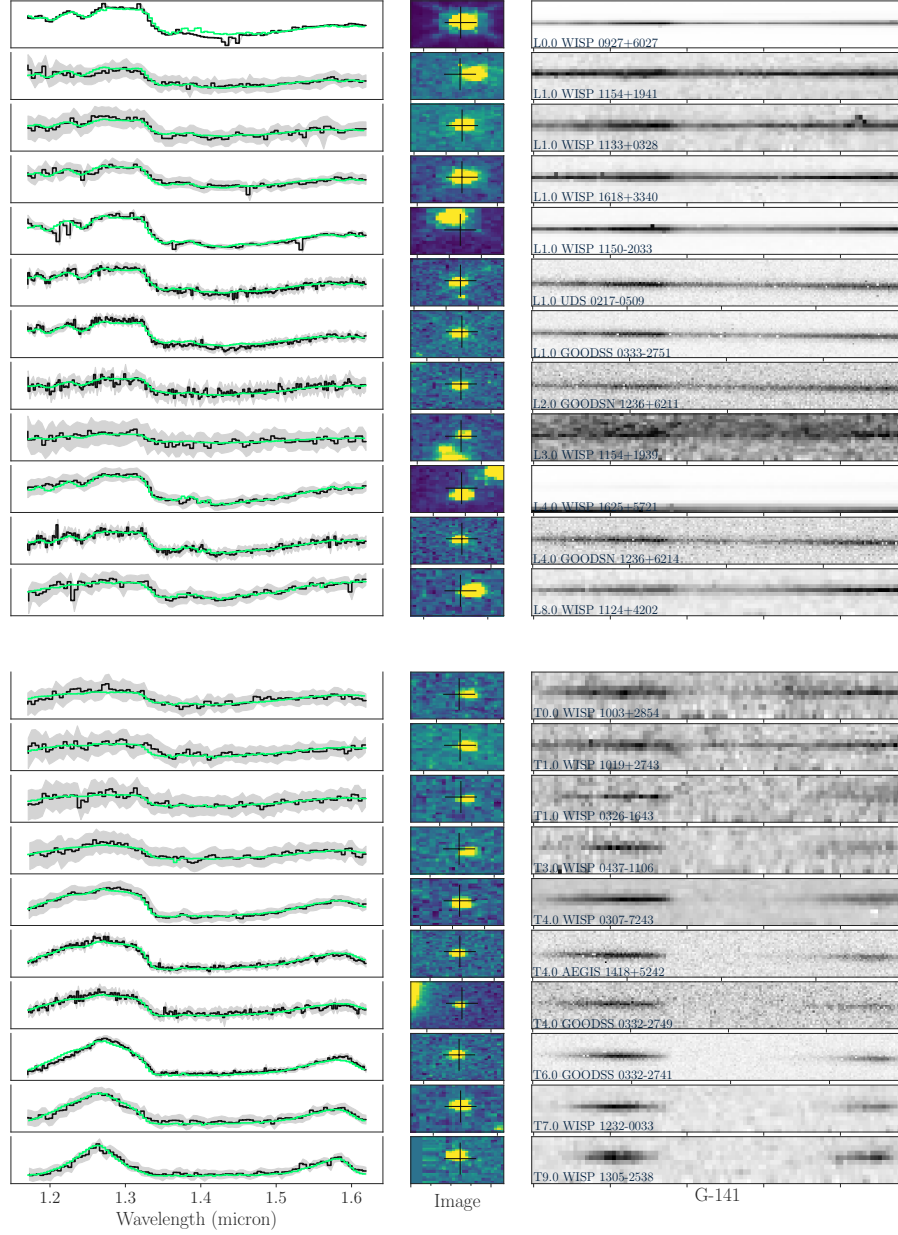
Figure 11. Spectral Sequence of UCDs Discovered in WISPS & 3D-HST. The right plot shows the 1D spectrum where the shaded region is the reported contamination by the survey, the middle plot shows the WFC3 image acquired in either F140W, F160W or F110W filter and the far-left plot shows the cutoff of the G141 spectrum for that extracted object. The derived spectral type of each object is displayed in the left corner of the far-left plot
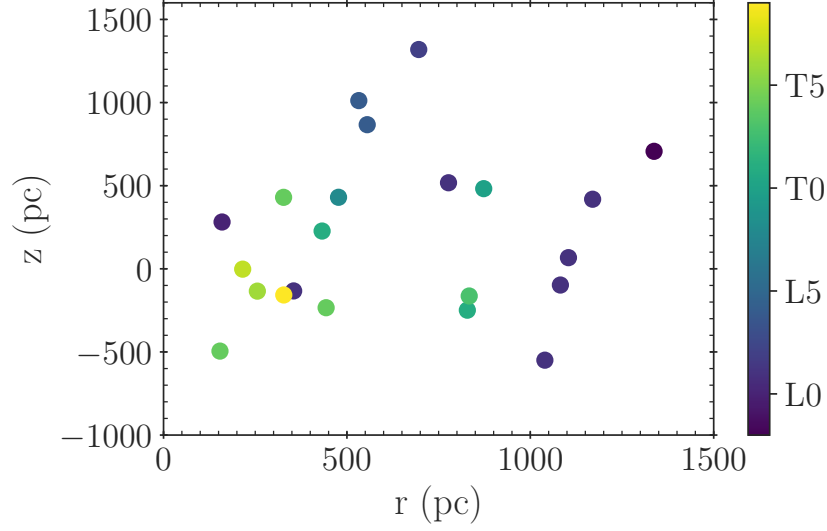
Figure 12. Spatial distribution of the the UCD sample reported in this paper

(a)

(b)
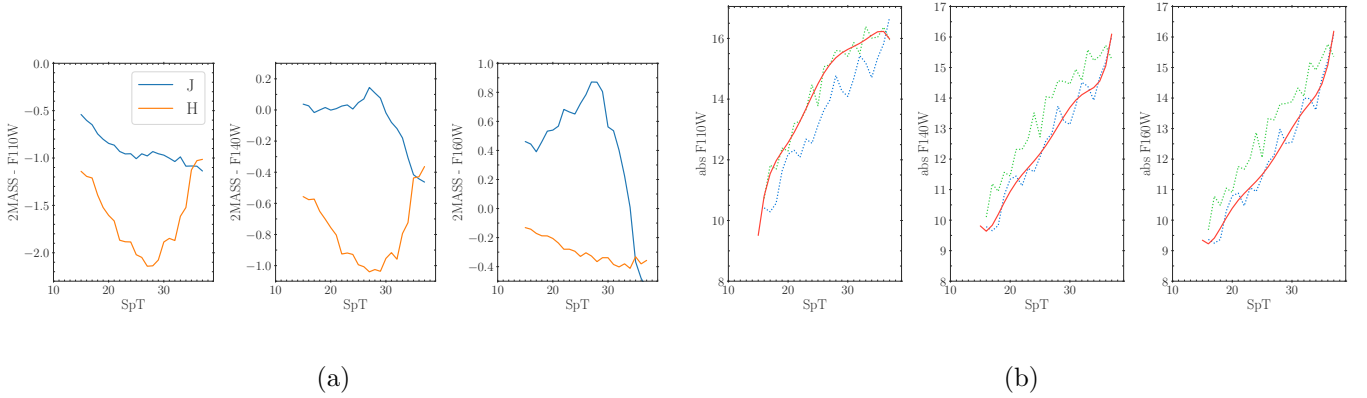
Figure 13. (a) Offsets between 2MASS J, H magnitudes and HST F110W, F140W, F160W magnitudes as a function of spectral type (b) Absolute magnitude-spectral type relations for HST and 2 MASS filters. For HST filters, the dotted green curve shows the derived relation using only the offset between the respective HST filter and 2MASS J filter while the blue curve shows the derived relation using the offset with the 2MASS H filter. The solid line shows a best-fit 6th-order polynomial used, considering the wavelength coverage of the respective filters (figure 6). We report the coefficients of these polynomials in table 3
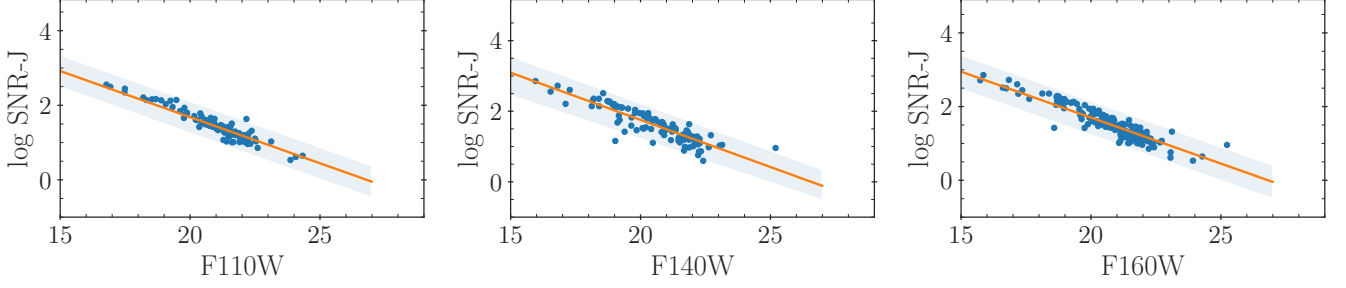
Figure 14. Linear fits between SNR-J and apparent F110W, F140W, F160W magnitudes using the sample of UCDs. These relations are reported in table 3 and used to estimate SNR-J for different apparent magnitudes
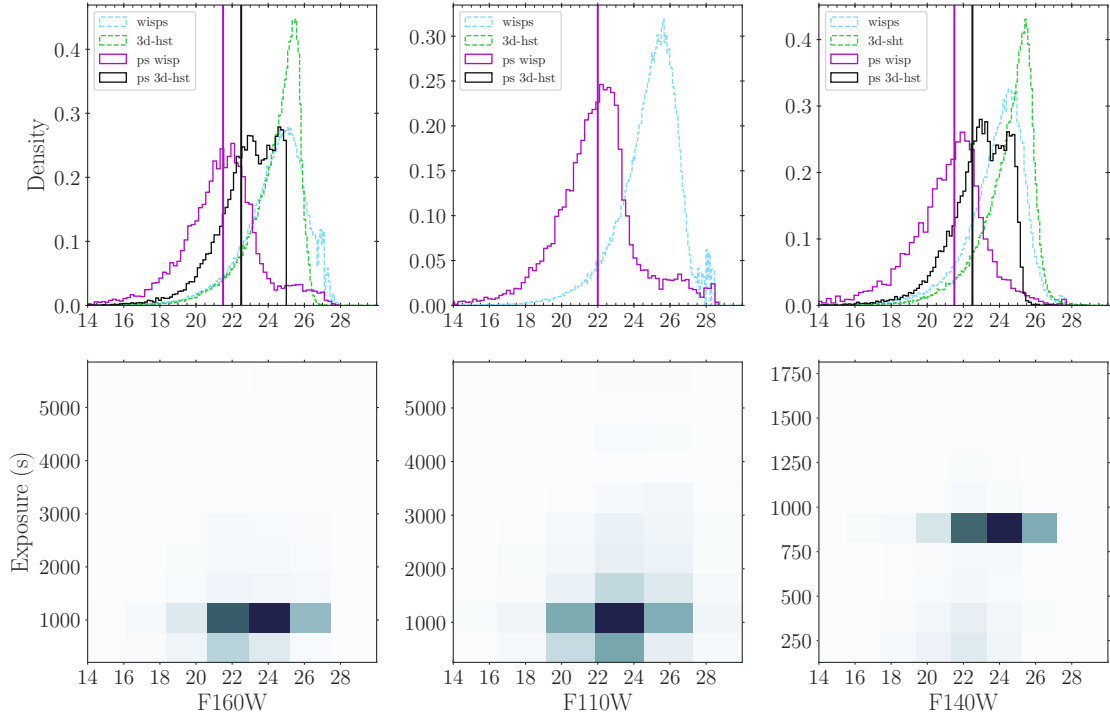
Figure 15. Magnitude distribution of point sources (solid lines) and all the sources (dotted lines) in both WISP & 3D-HST. We estimate the limiting magnitudes based on the distribution of point sources. For wisps the limiting magnitudes are F110W=22.0, F140W= 21.5, and F160W= 21.5. For 3D-HST the limiting magnitudes are F140W=22.5 and F160W. These magnitudes are used to compute the effective volumes for each spectral type
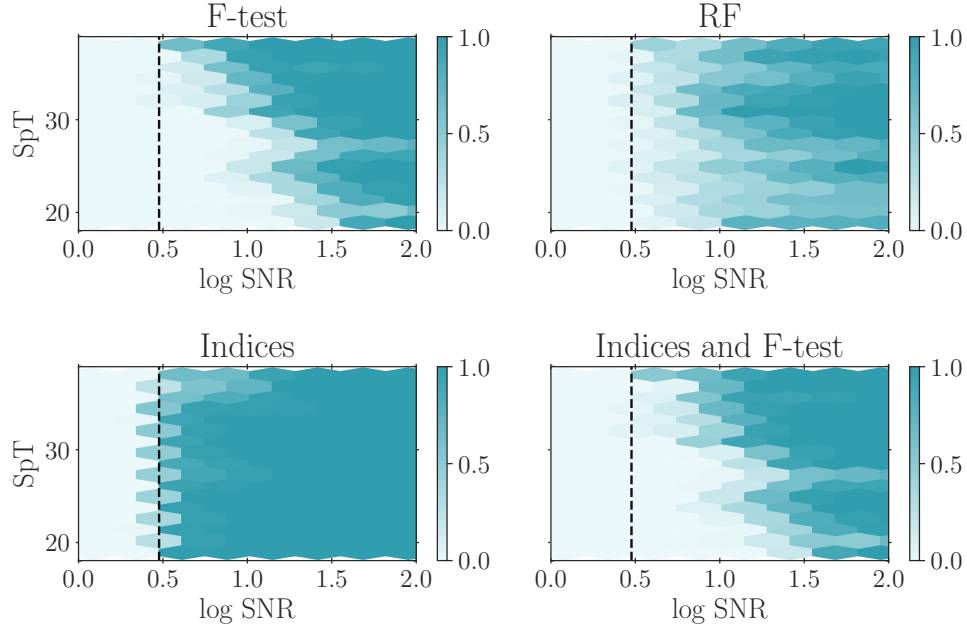
Figure 16. Visualization of our selection function as a function accross spectral type and SNR-J. The label "F-test" indicates spectra with F-test >0.5, the label "RF" indicates the spectra labelled as UCDs by the random forest classifier, and the label "Indices" indicates the spectra selected by our best selection criteria. The bar indicates the selection probability defined as the number of spectra selected over the total number of spectra in each SNR-J, spectral type bin. In the Monte-Carlo simulation, we use the most-selective selection function.
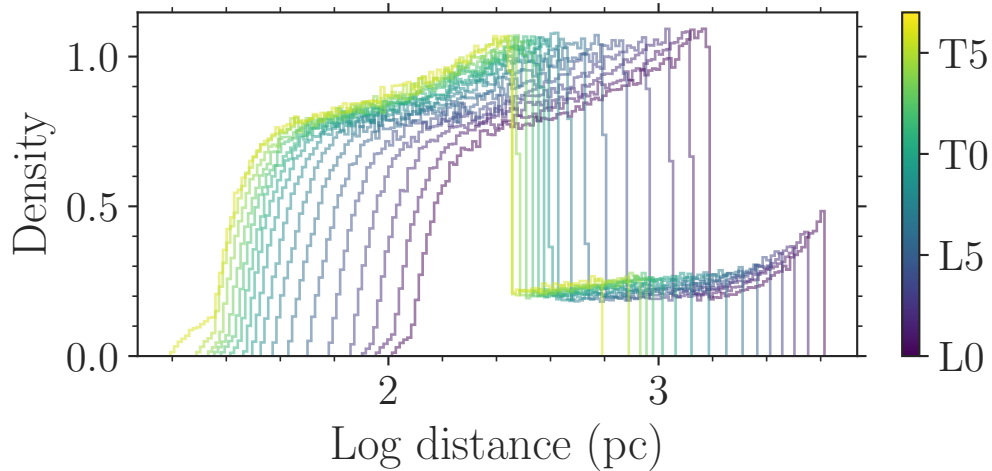
Figure 17. Distribution of randomly drawn distances in all WISPS & 3D-HST pointings 15
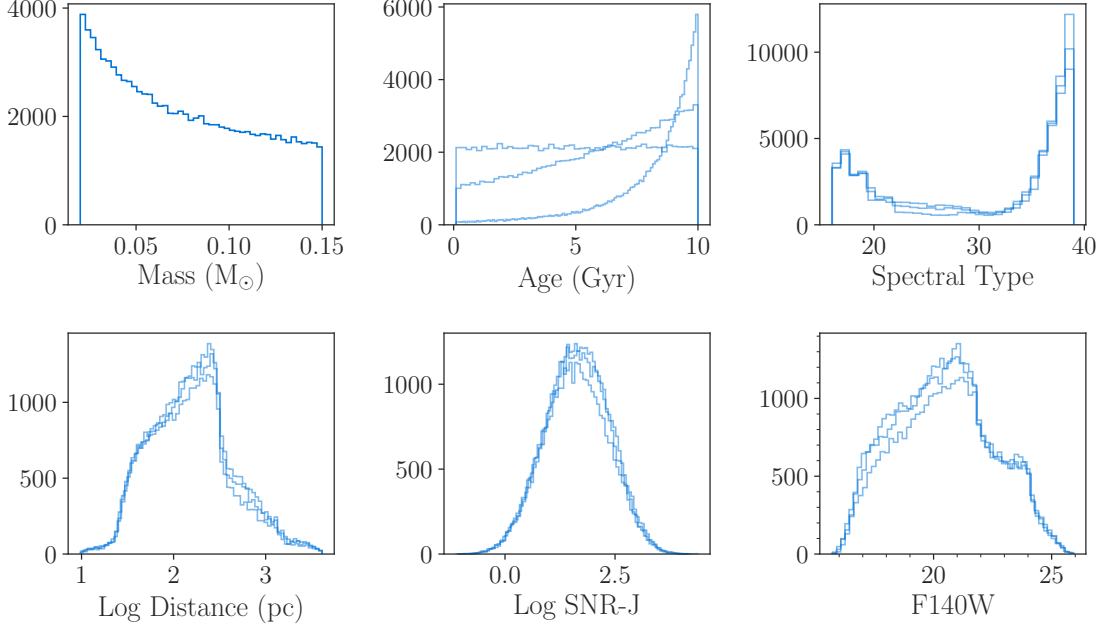
Figure 18. Monte-Carlo simulation: distribution of randomly drawn masses, ages, distances and computed spectral types, SNR-J and apparent F140W following relations defined in this work
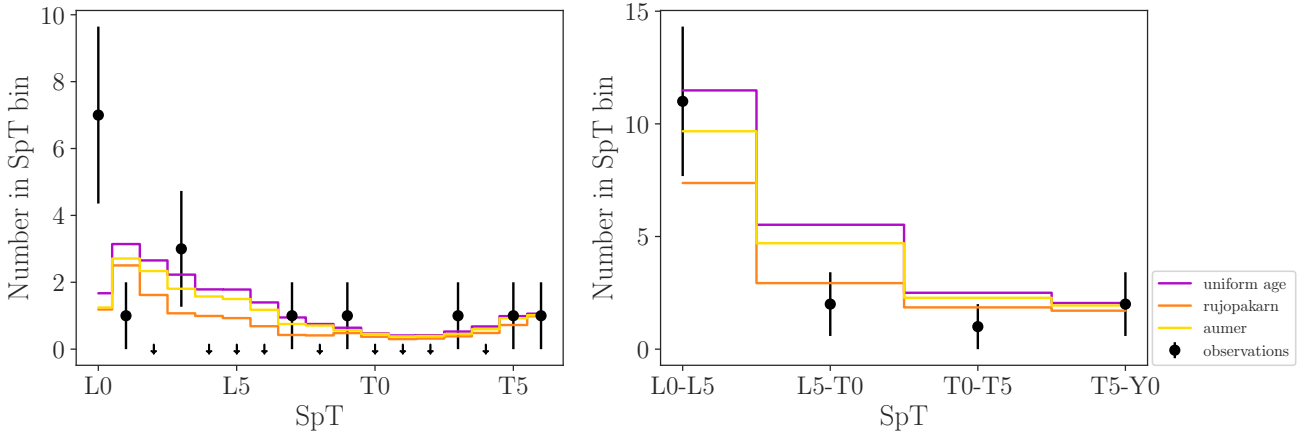
Figure 19. Comparison between the measured number densities and the expected number densities based on the Monte-Carlo simulation based on different age distirbutions. We observe an under-prediction within Poisson-like errorbars ($\sim \sqrt{N}$) between the predictions and the measurements per subtype but an agreement within subgroupings of 5 subtypes. The total number of predicted UCDs with spectral types $\geq$ L0 is 16.9 while the total number of UCDs within the limiting magnitudes (F110W >22.0 or F140W >21.5) is 16

Table 2. List of L0-T9 UCDs

Short Name	Grism ID	SNR-J	SpT	RA	DEC	F110W	F140W	F160W	Distance (pc)	Distance er
WISP0927+6027	PAR21-00005	324	L0	141.989319	60.462970		18.6		323	7
UDS0217-0509	UDS-25-G141_36758	31	L1	34.318333	-5.153692		21.3	21.0	1086	81
WISP1154+1941	PAR338-00035	13	L1	178.716644	19.684700	22.2		21.9	1242	532
WISP1133+0328	PAR27-00036	10	L1	173.274353	3.477643	21.6	22.0	21.4	1106	407
WISP1618+3340	PAR65-00035	19	L1	244.707458	33.671520	21.7		21.3	933	390
WISP1150-2033	PAR199-00009	57	L1	177.706833	-20.561000		19.2		379	7
WISP1004+5258	PAR438-00051	10	L1	151.204559	52.974800		22.6		1845	32
WISP0015-7955	PAR244-00072	6	L1	3.785810	-79.930220		22.2		1531	27
GOODSS0333-2751	GOODSS-28-G141_10859	34	L1	53.267498	-27.860249		21.4	21.3	1176	154
GOODSN1236+6211	GOODSN-33-G141_09283	12	L2	189.223923	62.188259		22.2	22.0	1491	130
WISP1154+1939	PAR338-00136	4	L3	178.720154	19.660000	24.1		23.1	1809	661
WISP1625+5721	PAR156-00041	19	L4	246.353882	57.357600			21.4	1029	14
GOODSN1236+6214	GOODSN-24-G141_21552	19	L4	189.161880	62.247669		22.0	21.8	1144	125
WISP1124+4202	PAR106-00047	11	L8	171.034760	42.042900			21.5	644	14
WISP1003+2854	PAR191-00077	6	T0	150.918884	28.912800			23.1	996	22
UDS0217-0514	UDS-12-G141_10759	9	T0	34.435657	-5.240000		25.2	25.2	2401	352
WISP0326-1643	PAR467-00135	3	T1	51.511295	-16.722500	23.9		23.9	865	444
WISP1019+2743	PAR201-00044	4	T1	154.888565	27.720400		22.4		489	7
WISP0437-1106	PAR463-00176	4	T3	69.490608	-11.104400	24.3		24.3	850	380
GOODSS0332-2749	GOODSS-04-G141_17402	13	T4	53.161709	-27.831562		22.6	22.9	501	69
WISP0307-7243	PAR130-00092	12	T4	46.921608	-72.732600			22.7	518	11
AEGIS1418+5242	AEGIS-03-G141_17053	21	T4	214.710007	52.716480		22.7	23.1	540	78
GOODSS0332-2741	GOODSS-01-G141_45889	31	T6	53.242542	-27.695446		22.1	22.9	289	52
WISP1232-0033	PAR58-00112	11	T7	188.176712	-0.551850		23.1		218	25
WISP1305-2538	PAR32-00075	11	T9	196.356232	-25.641300	23.1	23.0	22.7	359	495

Table 6. WISPS and 3D-HST Pointings

ra (deg)	dec(deg)	l (deg)	b (deg)	Exposure (s)	Observation Date (UT)	Pointing	Survey
214.887200	52.863000	96.439665	59.495788	406.0	2013-04-21	aegis-01	3d-hst
214.925811	52.835828	96.369843	59.500897	812.0	2011-05-03	aegis-02	3d-hst

Table 3. Polynomial relations used in this work where the polynomial is given by $y = \sum_{n=1}^{7} c_n x^n$

x	y	Scatter	Coefficients						
			c7	c6	c5	c4	c3	c2	c1
SpT	Abs F110W	0.4	-3.2×10^{-6}	5×10^{-4}	-3.4×10^{-2}	1.15	-2.2×10^{1}	2.2×10^{2}	-9×10^{2}
SpT	Abs F140W	0.4	3.5×10^{-6}	-5.4×10^{-4}	3.4×10^{-2}	-1.1	2×10^{1}	-2×10^{2}	7.85×10^{2}
SpT	Abs F160W	0.4	3×10^{-6}	-4.6×10^{-4}	2.9×10^{-2}	-0.96	1.8×10^{1}	-1.7×10^{2}	6.7×10^{2}
F110W	log SNR-J	0.42						-0.25	6.63
F140W	log SNR-J	0.46						-0.27	7.1
F160W	log SNR-J	0.45						-0.25	6.69

Table 4. Galaxy Model Parameters

Parameter	Description	Value	Reference
ρ_0	local UCD population	0.0055 pc^{-3}	Reid et al. (1999)
$R_\odot$	radial coordinate of the sun	8000 pc	Jurić et al. (2008)
$Z_\odot$	z coordinate of the sun	25 pc	Jurić et al. (2008)
H_{thick}	thick disk scale height	900 pc	Jurić et al. (2008)
H_{thin}	thin disk scale height	300 pc	Jurić et al. (2008)
L_{thick}	thick disk scale length	3600 pc	Jurić et al. (2008)
L_{thin}	thin disk scale length	2600 pc	Jurić et al. (2008)
p	halo power law index	2.77	Jurić et al. (2008)
q	halo sphere flattening parameter	0.64	Jurić et al. (2008)
f_{thick}	relative number of thick disk stars	0.12	Jurić et al. (2008)
f_{halo}	relative number of halo stars	0.0051	Jurić et al. (2008)

Table 6 *(continued)*

ra (deg)	dec(deg)	l (deg)	b (deg)	Exposure (s)	Observation Date (UT)	Pointing	Survey
214.696088	52.727431	96.435995	59.673916	812.0	2011-06-13	aegis-03	3d-hst
214.726055	52.795186	96.496768	59.610858	812.0	2011-03-16	aegis-04	3d-hst
214.684229	52.764025	96.494204	59.650975	812.0	2011-03-16	aegis-05	3d-hst

Table 5. Number Densities. Nex1 is the expected number with a uniform age distribution without selection effects, Nex2 is the expected number with a uniform age distribution taking selection effects into account and Nobs is the number in UCDs with that spectral type in the sample

SpT	Volume (pc^3)	Nex1	Nex2	Nobs
L0	13399.0	22.1	4.1	8
L1	10935.0	17.0	8.9	1
L2	8859.0	11.6	6.4	0
L3	7177.0	9.4	4.6	4
L4	5840.0	7.3	4.3	0
L5	4753.0	5.4	3.4	0
L6	3828.0	4.3	2.0	0
L7	3025.0	3.3	1.0	1
L8	2346.0	2.5	0.8	0
L9	1806.0	1.6	0.7	1
T0	1411.0	1.0	0.6	0
T1	1142.0	0.8	0.5	0
T2	969.0	0.9	0.5	0
T3	854.0	1.1	0.5	1
T4	753.0	1.5	0.7	0
T5	611.0	1.9	1.0	1
T6	400.0	2.0	1.1	1

Table 6 *(continued)*

ra (deg)	dec(deg)	l (deg)	b (deg)	Exposure (s)	Observation Date (UT)	Pointing	Survey
215.004656	52.878008	96.354122	59.437795	812.0	2011-10-11	aegis-06	3d-hst

Table 6 *(continued)*

ra (deg)	dec(deg)	l (deg)	b (deg)	Exposure (s)	Observation Date (UT)	Pointing	Survey
215.041584	52.905306	96.356632	59.402583	812.0	2011-10-30	aegis-07	3d-hst
214.997008	52.932625	96.431719	59.399772	812.0	2011-10-24	aegis-08	3d-hst
214.787740	52.787664	96.431374	59.592067	812.0	2011-06-20	aegis-09	3d-hst
214.965725	52.905728	96.424788	59.432434	812.0	2011-10-23	aegis-10	3d-hst
214.757533	52.721028	96.372083	59.654322	812.0	2011-06-18	aegis-12	3d-hst
214.757738	52.782711	96.452002	59.607714	812.0	2011-08-31	aegis-13	3d-hst
214.822015	52.819525	96.441838	59.554432	812.0	2011-06-27	aegis-14	3d-hst
214.806549	52.755792	96.373036	59.608616	812.0	2011-06-21	aegis-15	3d-hst
214.793452	52.737464	96.361020	59.627638	812.0	2011-09-03	aegis-18	3d-hst
214.925982	52.933969	96.496805	59.426933	812.0	2011-10-27	aegis-19	3d-hst
214.961388	52.858819	96.367854	59.469445	812.0	2011-10-28	aegis-21	3d-hst
214.821237	52.848256	96.479758	59.533073	812.0	2011-12-02	aegis-23	3d-hst
214.714420	52.760694	96.462574	59.641522	812.0	2011-09-02	aegis-24	3d-hst
214.746512	52.752603	96.423069	59.634890	812.0	2011-06-20	aegis-25	3d-hst
215.080781	52.928044	96.351268	59.369900	812.0	2011-10-28	aegis-26	3d-hst
215.000500	52.981036	96.491201	59.361954	812.0	2011-10-28	aegis-27	3d-hst
214.849741	52.788356	96.376462	59.566901	812.0	2011-06-27	aegis-28	3d-hst
214.843668	52.895481	96.520714	59.488556	812.0	2011-05-02	aegis-11	3d-hst
150.072500	2.400000	236.572289	42.196083	812.0	2011-04-16	cosmos-01	3d-hst
150.077782	2.333333	236.649796	42.161828	812.0	2011-04-06	cosmos-03	3d-hst
150.176788	2.303889	236.759537	42.225410	812.0	2011-06-05	cosmos-04	3d-hst
150.071944	2.261667	236.724031	42.115569	812.0	2011-06-05	cosmos-05	3d-hst
150.074029	2.225833	236.765015	42.096495	812.0	2011-06-09	cosmos-06	3d-hst
150.069718	2.436111	236.530334	42.214681	812.0	2011-06-09	cosmos-07	3d-hst
150.104912	2.451389	236.540923	42.252207	812.0	2011-06-10	cosmos-08	3d-hst
150.172208	2.339167	236.717126	42.242126	812.0	2011-06-11	cosmos-09	3d-hst
150.113115	2.347778	236.661475	42.198977	812.0	2012-03-09	cosmos-10	3d-hst

Table 6 continued on next page

Table 6 *(continued)*

ra (deg)	dec(deg)	l (deg)	b (deg)	Exposure (s)	Observation Date (UT)	Pointing	Survey
150.139808	2.466389	236.551599	42.289330	812.0	2011-06-17	cosmos-11	3d-hst
150.106165	2.277222	236.733657	42.152450	812.0	2011-06-17	cosmos-12	3d-hst
150.108389	2.241250	236.774924	42.133406	812.0	2011-06-12	cosmos-13	3d-hst
150.107972	2.204306	236.815170	42.111634	812.0	2011-06-12	cosmos-14	3d-hst
150.145348	2.429722	236.596365	42.272653	812.0	2010-11-03	cosmos-15	3d-hst
150.146597	2.395000	236.635613	42.253588	812.0	2010-10-30	cosmos-16	3d-hst
150.150829	2.363611	236.673498	42.238869	812.0	2010-11-03	cosmos-17	3d-hst
150.170953	2.373056	236.678822	42.260732	812.0	2011-03-27	cosmos-18	3d-hst
150.171882	2.226111	236.841214	42.176294	812.0	2012-03-02	cosmos-19	3d-hst
150.149375	2.325278	236.714564	42.215484	812.0	2010-11-03	cosmos-20	3d-hst
150.143124	2.256111	236.785748	42.170300	812.0	2011-06-12	cosmos-21	3d-hst
150.178985	2.263333	236.805863	42.203677	812.0	2012-03-04	cosmos-22	3d-hst
150.141456	2.290833	236.746269	42.189075	812.0	2011-04-07	cosmos-23	3d-hst
150.113250	2.311389	236.701621	42.178016	812.0	2010-11-03	cosmos-24	3d-hst
150.111167	2.379722	236.624783	42.215875	812.0	2010-12-11	cosmos-25	3d-hst
150.077083	2.297500	236.688660	42.140513	812.0	2010-11-03	cosmos-26	3d-hst
150.076668	2.364167	236.614996	42.178761	812.0	2010-11-03	cosmos-27	3d-hst
150.110891	2.413611	236.587233	42.235250	812.0	2010-11-04	cosmos-28	3d-hst
150.142317	2.219028	236.825861	42.148127	812.0	2011-05-27	cosmos-02	3d-hst
34.472436	-5.174425	169.944196	-59.901920	812.0	2011-11-28	uds-01	3d-hst
34.472456	-5.211917	169.993139	-59.930270	812.0	2011-11-30	uds-02	3d-hst
34.472435	-5.249411	170.042107	-59.958631	812.0	2011-11-30	uds-03	3d-hst
34.438964	-5.173997	169.893301	-59.923378	812.0	2011-12-04	uds-04	3d-hst
34.373292	-5.144000	169.755299	-59.943315	812.0	2011-08-20	uds-05	3d-hst
34.387072	-5.192750	169.839581	-59.971323	812.0	2011-08-27	uds-06	3d-hst
34.369374	-5.223444	169.852938	-60.006082	812.0	2012-01-23	uds-07	3d-hst
34.340221	-5.208047	169.788823	-60.013354	812.0	2012-01-13	uds-08	3d-hst

Table 6 *(continued)*

ra (deg)	dec(deg)	l (deg)	b (deg)	Exposure (s)	Observation Date (UT)	Pointing	Survey
34.318896	-5.238872	169.796836	-60.050571	812.0	2012-01-14	uds-09	3d-hst
34.348577	-5.254700	169.862379	-60.043278	812.0	2012-01-14	uds-10	3d-hst
34.438966	-5.211358	169.942037	-59.951659	812.0	2011-11-22	uds-11	3d-hst
34.438526	-5.249272	169.990915	-59.980627	812.0	2011-11-24	uds-12	3d-hst
34.357367	-5.178444	169.776117	-59.979775	812.0	2011-08-27	uds-13	3d-hst
34.405083	-5.249694	169.941093	-60.002727	812.0	2011-12-01	uds-14	3d-hst
34.266570	-5.230681	169.706939	-60.078317	812.0	2012-01-20	uds-15	3d-hst
34.405055	-5.212478	169.892429	-59.974574	812.0	2011-12-21	uds-17	3d-hst
34.583333	-5.170833	170.105831	-59.826913	812.0	2012-01-28	uds-18	3d-hst
34.245104	-5.178714	169.606648	-60.052765	812.0	2012-01-14	uds-20	3d-hst
34.237403	-5.214967	169.642220	-60.085292	812.0	2012-01-20	uds-21	3d-hst
34.246752	-5.254425	169.707916	-60.109188	812.0	2012-01-20	uds-22	3d-hst
34.260595	-5.149978	169.592723	-60.020899	812.0	2011-08-20	uds-23	3d-hst
34.405046	-5.173589	169.841697	-59.945123	812.0	2011-12-16	uds-24	3d-hst
34.336872	-5.143169	169.699247	-59.966311	812.0	2011-08-23	uds-25	3d-hst
34.294525	-5.155247	169.650945	-60.002929	812.0	2011-08-23	uds-26	3d-hst
34.277876	-5.190108	169.671142	-60.040190	812.0	2011-08-28	uds-27	3d-hst
34.371991	-5.250667	169.892456	-60.024997	812.0	2011-12-21	uds-28	3d-hst
34.291690	-5.250814	169.771280	-60.077291	812.0	2012-01-14	uds-16	3d-hst
34.320952	-5.177056	169.719302	-60.002353	812.0	2011-08-28	uds-19	3d-hst
188.979083	62.197583	126.073735	54.835883	812.0	2010-04-15	goodsn-11	3d-hst
188.979083	62.197583	126.073735	54.835883	203.0	2011-04-19	goodsn-111	3d-hst
189.122208	62.264278	125.946774	54.776380	406.0	2011-04-20	goodsn-114	3d-hst
189.026792	62.219806	126.031321	54.816092	812.0	2010-04-15	goodsn-12	3d-hst
189.074542	62.242056	125.988964	54.796242	812.0	2010-04-15	goodsn-13	3d-hst
189.122208	62.264278	125.946774	54.776380	812.0	2010-04-16	goodsn-14	3d-hst
189.169917	62.286528	125.904641	54.756459	812.0	2010-04-22	goodsn-15	3d-hst

Table 6 *(continued)*

ra (deg)	dec(deg)	l (deg)	b (deg)	Exposure (s)	Observation Date (UT)	Pointing	Survey
189.217583	62.308750	125.862642	54.736530	812.0	2010-09-25	goodsn-16	3d-hst
189.313042	62.353194	125.778827	54.696575	812.0	2010-09-26	goodsn-18	3d-hst
189.128958	62.216667	125.949653	54.824066	812.0	2010-04-17	goodsn-23	3d-hst
189.176667	62.238917	125.907412	54.804147	812.0	2010-04-17	goodsn-24	3d-hst
189.224375	62.261139	125.865271	54.784221	812.0	2010-04-22	goodsn-25	3d-hst
189.272083	62.283361	125.823225	54.764262	812.0	2010-09-21	goodsn-26	3d-hst
189.319792	62.305611	125.781270	54.744240	812.0	2009-09-16	goodsn-27	3d-hst
189.367500	62.327833	125.739415	54.724213	812.0	2009-09-16	goodsn-28	3d-hst
189.088000	62.146833	125.994961	54.891608	812.0	2010-04-18	goodsn-31	3d-hst
189.135750	62.169056	125.952487	54.871755	812.0	2010-04-18	goodsn-32	3d-hst
189.231167	62.213528	125.867889	54.831914	812.0	2010-04-20	goodsn-34	3d-hst
189.278833	62.235750	125.825769	54.811954	812.0	2009-09-25	goodsn-35	3d-hst
189.326542	62.258000	125.783706	54.791934	812.0	2010-04-23	goodsn-36	3d-hst
189.142458	62.121444	125.955378	54.919440	812.0	2010-03-07	goodsn-41	3d-hst
189.190208	62.143694	125.912887	54.899527	812.0	2010-04-19	goodsn-42	3d-hst
189.237875	62.165917	125.870563	54.879603	812.0	2010-04-21	goodsn-43	3d-hst
189.285625	62.188139	125.828268	54.859648	812.0	2010-04-21	goodsn-44	3d-hst
189.333292	62.210389	125.786131	54.839629	812.0	2010-04-09	goodsn-45	3d-hst
189.381042	62.232611	125.744027	54.819606	812.0	2010-04-23	goodsn-46	3d-hst
53.257475	-27.689022	223.402881	-54.296285	812.0	2011-11-27	goodss-01	3d-hst
53.065672	-27.807456	223.560145	-54.481905	812.0	2011-10-18	goodss-02	3d-hst
53.152490	-27.686917	223.375077	-54.387849	812.0	2011-10-13	goodss-03	3d-hst
53.156682	-27.841800	223.639076	-54.407399	812.0	2012-03-22	goodss-04	3d-hst
53.087237	-27.904864	223.730809	-54.477399	812.0	2012-03-20	goodss-05	3d-hst
53.210821	-27.859708	223.681655	-54.362709	812.0	2011-03-23	goodss-06	3d-hst
53.192388	-27.801433	223.578583	-54.370172	812.0	2011-10-13	goodss-08	3d-hst
53.066020	-27.772556	223.500824	-54.476406	812.0	2012-01-22	goodss-09	3d-hst

Table 6 continued on next page

Table 6 *(continued)*

ra (deg)	dec(deg)	l (deg)	b (deg)	Exposure (s)	Observation Date (UT)	Pointing	Survey
53.116617	-27.855642	223.653607	-54.444481	812.0	2012-03-21	goodss-10	3d-hst
53.148988	-27.710939	223.415052	-54.394552	812.0	2012-01-22	goodss-11	3d-hst
53.069622	-27.735247	223.438166	-54.467667	812.0	2012-01-22	goodss-12	3d-hst
53.130920	-27.886942	223.710044	-54.436582	812.0	2012-03-21	goodss-13	3d-hst
53.185354	-27.904864	223.752644	-54.391626	812.0	2012-03-22	goodss-14	3d-hst
53.105559	-27.932422	223.781790	-54.465405	812.0	2012-03-21	goodss-15	3d-hst
53.145517	-27.918558	223.767062	-54.428454	812.0	2012-03-22	goodss-16	3d-hst
53.105478	-27.762256	223.492283	-54.440344	812.0	2012-01-28	goodss-17	3d-hst
53.190962	-27.767136	223.520050	-54.366287	812.0	2011-09-30	goodss-18	3d-hst
53.068688	-27.841336	223.618501	-54.484284	812.0	2011-10-16	goodss-19	3d-hst
53.110366	-27.829419	223.607602	-54.446071	812.0	2011-10-20	goodss-20	3d-hst
53.170750	-27.873189	223.695568	-54.399735	812.0	2012-03-22	goodss-21	3d-hst
53.225016	-27.891378	223.738587	-54.354972	812.0	2012-03-22	goodss-22	3d-hst
53.036152	-27.755931	223.465726	-54.500055	812.0	2011-06-02	goodss-24	3d-hst
53.040975	-27.795044	223.533427	-54.501666	812.0	2011-12-04	goodss-25	3d-hst
53.086650	-27.868953	223.669543	-54.472646	812.0	2011-06-22	goodss-26	3d-hst
53.196488	-27.828264	223.625054	-54.370581	812.0	2011-04-04	goodss-27	3d-hst
53.272613	-27.857072	223.691060	-54.308291	812.0	2011-02-15	goodss-28	3d-hst
53.185307	-27.735033	223.464282	-54.366407	812.0	2012-01-24	goodss-29	3d-hst
53.109115	-27.724794	223.429436	-54.431536	812.0	2012-01-30	goodss-30	3d-hst
53.107613	-27.795386	223.549101	-54.443423	812.0	2011-10-24	goodss-31	3d-hst
53.149228	-27.781083	223.534234	-54.404886	812.0	2011-10-19	goodss-32	3d-hst
53.145491	-27.748414	223.477890	-54.403259	812.0	2012-01-29	goodss-33	3d-hst
53.162025	-27.781733	223.538246	-54.393788	812.0	2011-08-20	goodss-34	3d-hst
53.110917	-27.700703	223.388909	-54.426323	812.0	2011-10-20	goodss-35	3d-hst
53.165138	-27.780500	223.536859	-54.390881	812.0	2011-08-22	goodss-36	3d-hst
53.161083	-27.783500	223.541033	-54.394876	812.0	2011-08-24	goodss-37	3d-hst

Table 6 *(continued)*

ra (deg)	dec(deg)	l (deg)	b (deg)	Exposure (s)	Observation Date (UT)	Pointing	Survey
53.164308	-27.783133	223.541142	-54.392000	812.0	2011-08-29	goodss-38	3d-hst
189.265333	62.330972	125.820670	54.716570	812.0	2009-09-23	goodsn-17	3d-hst
189.033542	62.172222	126.034411	54.863746	812.0	2010-04-16	goodsn-21	3d-hst
189.081250	62.194444	125.991984	54.843924	812.0	2010-04-16	goodsn-22	3d-hst
189.183417	62.191306	125.910171	54.851836	812.0	2010-04-19	goodsn-33	3d-hst
53.149857	-27.812683	223.588063	-54.409047	812.0	2011-10-13	goodss-07	3d-hst
189.128958	62.216667	125.949653	54.824066	406.0	2011-04-22	goodsn-123	3d-hst
162.271429	2.249768	248.026996	51.577923	1265.0	2014-04-09	par334	3d-hst
16.645713	15.146204	128.352543	-47.566081	884.0	2009-11-24	par1	3d-hst
141.284864	48.952821	169.613897	45.000578	631.0	2010-01-02	par10	3d-hst
208.352864	3.496558	337.683916	62.111596	734.0	2011-03-11	par101	3d-hst
109.638781	74.429665	140.480493	27.868897	581.0	2011-03-19	par103	3d-hst
151.354699	1.495416	238.584522	42.701995	2976.0	2011-03-11	par104	3d-hst
230.083706	-24.999888	340.795503	26.716198	709.0	2011-04-09	par105	wisps
171.037498	42.038962	167.366366	66.775092	356.0	2011-04-25	par106	wisps
200.478538	46.809950	107.969310	69.422968	734.0	2011-04-26	par107	wisps
182.693527	36.957706	161.569611	76.945426	734.0	2011-04-27	par108	wisps
165.574797	10.907745	239.948688	59.650861	556.0	2010-01-03	par11	wisps
194.244995	54.521869	121.185176	62.587583	684.0	2011-05-09	par110	wisps
349.071230	-42.492952	348.309375	-65.299716	456.0	2011-05-10	par111	wisps
160.239956	6.123961	241.093271	52.558621	1137.0	2011-05-27	par114	wisps
169.727620	2.284413	257.265992	56.716032	912.0	2011-05-28	par115	wisps
161.703821	13.041686	232.515955	57.658300	909.0	2011-05-30	par116	wisps
169.380325	26.532604	209.179061	69.070411	734.0	2011-06-02	par119	wisps
182.358212	45.723468	144.359578	69.617510	1312.0	2010-01-04	par12	wisps
209.212278	17.041716	2.600531	71.827499	837.0	2011-06-10	par120	wisps
180.402367	-13.944577	284.991352	47.184009	659.0	2011-07-25	par121	wisps

Table 6 (continued)

ra (deg)	dec(deg)	l (deg)	b (deg)	Exposure (s)	Observation Date (UT)	Pointing	Survey
230.288221	59.674864	95.267707	48.628083	431.0	2011-06-12	par122	wisps
222.680543	27.161772	39.929405	63.527232	734.0	2011-06-18	par123	wisps
278.115350	53.749422	82.654344	24.283278	456.0	2011-06-21	par124	wisps
259.222959	66.050316	96.224144	34.164608	556.0	2011-06-22	par125	wisps
205.436952	5.062026	333.669161	64.887470	762.0	2011-06-27	par126	wisps
40.838250	-72.187316	291.721964	-42.419757	406.0	2011-06-29	par127	wisps
20.690610	-28.634566	227.023265	-82.917439	815.0	2011-06-29	par128	wisps
165.575724	20.867628	221.122240	64.358222	687.0	2011-06-30	par129	wisps
16.660599	15.138351	128.374774	-47.572649	556.0	2010-01-07	par13	wisps
46.923242	-72.740371	290.238642	-40.859258	406.0	2011-06-30	par130	wisps
171.580220	-1.723657	264.150773	54.609151	634.0	2011-07-03	par132	wisps
323.463521	-49.085984	349.050081	-46.380394	406.0	2011-07-10	par133	wisps
281.879869	-68.978629	326.213318	-24.845854	506.0	2011-07-14	par134	wisps
170.598751	57.847041	143.796987	55.526149	862.0	2011-07-15	par135	wisps
186.617875	5.383250	286.532423	67.456622	3035.0	2011-06-11	par136	wisps
255.180138	29.377388	51.017836	35.728451	456.0	2011-07-18	par137	wisps
236.386667	9.567010	18.237367	45.405548	762.0	2011-07-19	par138	wisps
205.608506	18.699485	359.896377	75.561397	734.0	2011-07-22	par139	wisps
38.735563	-4.117314	174.508211	-56.245951	834.0	2010-01-09	par14	wisps
208.852036	0.777992	335.809044	59.503010	709.0	2011-07-26	par140	wisps
223.568209	16.172510	18.235285	59.532153	584.0	2011-07-27	par141	wisps
210.589497	9.763290	350.214565	65.889967	1568.0	2011-07-24	par143	wisps
196.299717	-10.592445	308.446027	52.131911	459.0	2011-08-16	par144	wisps
30.515698	-11.452537	172.965376	-67.178382	684.0	2011-08-17	par145	wisps
33.115938	-7.536832	171.088538	-62.565671	734.0	2011-08-21	par146	wisps
359.582181	-10.248989	83.859087	-68.988566	784.0	2011-08-23	par147	wisps
241.364981	25.798059	42.636118	46.830675	790.0	2011-09-01	par148	wisps

Table 6 *(continued)*

ra (deg)	dec(deg)	l (deg)	b (deg)	Exposure (s)	Observation Date (UT)	Pointing	Survey
65.473613	14.365499	180.503291	-24.227070	634.0	2011-09-16	par149	wisps
212.428972	26.367222	34.900906	72.525515	1612.0	2010-02-12	par15	wisps
62.753827	18.374451	175.315780	-23.600769	634.0	2011-09-16	par150	wisps
232.111763	28.345703	44.283565	55.390411	712.0	2011-09-17	par151	wisps
223.151553	31.624885	49.944185	63.310366	709.0	2011-09-23	par152	wisps
353.412188	39.420877	106.937921	-21.022739	684.0	2011-09-25	par153	wisps
239.237552	63.747870	97.018887	42.885665	481.0	2011-10-05	par154	wisps
255.795925	61.599041	91.171838	36.420027	481.0	2011-10-05	par155	wisps
246.353080	57.363627	87.227746	42.030958	481.0	2011-10-17	par156	wisps
226.287426	56.733351	93.491129	52.063640	481.0	2011-10-19	par157	wisps
234.575262	57.511378	90.745319	47.855735	203.0	2011-10-19	par158	wisps
314.123046	-4.804235	43.653270	-29.897424	734.0	2011-10-20	par159	wisps
38.726638	-4.111805	174.489822	-56.248233	1087.0	2010-02-16	par16	wisps
225.027015	53.235153	89.459537	54.706636	456.0	2011-10-21	par160	wisps
242.929429	52.362923	81.257824	45.228698	684.0	2011-10-21	par161	wisps
254.877089	37.497546	60.899309	37.507931	153.0	2011-10-29	par162	wisps
155.775328	39.549332	181.317055	56.908516	153.0	2011-10-29	par163	wisps
346.798882	21.190597	92.726302	-35.494011	406.0	2011-11-02	par165	wisps
346.816933	21.205759	92.753375	-35.488789	406.0	2011-11-02	par166	wisps
25.348670	13.624747	141.050429	-47.481868	659.0	2011-11-07	par167	wisps
24.203208	41.492269	131.986595	-20.580333	278.0	2011-11-09	par168	wisps
165.959947	-32.787984	278.149701	24.854271	456.0	2011-11-09	par169	wisps
33.407710	12.914257	152.015508	-45.265510	559.0	2010-02-18	par17	wisps
151.733481	-29.889687	265.363241	20.731793	456.0	2011-11-20	par170	wisps
151.733481	-29.889687	265.363241	20.731793	456.0	2011-11-20	par171	wisps
303.744824	-26.983476	15.654859	-29.316603	253.0	2011-11-28	par172	wisps
28.858483	-9.043603	165.825744	-66.427545	759.0	2011-12-04	par173	wisps

Table 6 continued on next page

Table 6 *(continued)*

ra (deg)	dec(deg)	l (deg)	b (deg)	Exposure (s)	Observation Date (UT)	Pointing	Survey
234.314937	54.530714	86.817091	49.324637	456.0	2011-12-18	par174	wisps
55.570091	-20.560566	212.828344	-50.573312	353.0	2012-01-06	par175	wisps
55.574795	-20.513689	212.760366	-50.554543	353.0	2012-01-06	par176	wisps
176.804296	-14.086987	280.243891	45.936569	178.0	2012-01-06	par177	wisps
156.175035	-18.730245	261.101012	31.971349	253.0	2012-01-21	par179	wisps
187.323753	10.735116	284.239832	72.798330	534.0	2010-02-19	par18	wisps
189.112141	26.732400	218.837826	86.635796	862.0	2012-01-29	par181	wisps
352.443381	25.526752	100.674535	-33.790975	203.0	2012-01-29	par182	wisps
173.820004	25.985372	212.447855	72.947304	837.0	2012-02-01	par183	wisps
200.930021	34.587399	82.054983	79.827687	153.0	2012-02-15	par186	wisps
120.626022	18.969924	202.997941	23.894175	253.0	2012-02-23	par188	wisps
75.549759	7.521417	192.743611	-20.189532	406.0	2012-02-26	par189	wisps
38.724804	-4.110487	174.485810	-56.248569	1187.0	2010-02-20	par19	wisps
70.221178	-43.287746	248.057574	-41.456626	203.0	2012-03-10	par190	wisps
150.903558	28.921873	200.070515	53.113261	459.0	2012-03-11	par191	wisps
147.738464	35.739548	188.715186	50.901682	406.0	2012-03-18	par192	wisps
154.080895	59.417619	151.495623	48.206370	178.0	2012-04-03	par193	wisps
73.948947	-22.032086	222.000246	-34.742551	128.0	2012-04-04	par194	wisps
201.975506	52.811159	110.567930	63.432979	178.0	2012-04-05	par195	wisps
172.812391	15.976361	239.784745	68.322450	406.0	2012-04-07	par196	wisps
309.607258	-20.356937	24.963506	-32.286721	178.0	2012-04-08	par197	wisps
15.018843	-51.158709	299.612438	-65.913837	178.0	2012-04-10	par198	wisps
177.711506	-20.565399	284.277709	40.101360	203.0	2012-04-19	par199	wisps
21.290377	21.651712	133.262269	-40.542611	328.0	2009-12-12	par2	wisps
212.423320	26.372645	34.916813	72.531195	1815.0	2010-02-15	par20	wisps
160.651752	7.779520	239.301711	53.884430	303.0	2012-04-20	par200	wisps
154.885213	27.703906	202.987017	56.421411	153.0	2012-04-20	par201	wisps

Table 6 *(continued)*

ra (deg)	dec(deg)	l (deg)	b (deg)	Exposure (s)	Observation Date (UT)	Pointing	Survey
168.694909	2.596904	255.473990	56.286951	406.0	2012-04-24	par202	wisps
329.268475	22.781489	78.529407	-24.692571	153.0	2012-04-24	par203	wisps
169.943008	4.170147	255.295266	58.291445	253.0	2012-04-27	par204	wisps
188.898421	-39.835177	299.629981	22.934967	278.0	2012-04-28	par205	wisps
158.592558	-28.519394	269.732563	25.375262	381.0	2012-05-06	par206	wisps
204.916615	-0.052155	327.992065	60.451587	178.0	2012-05-18	par209	wisps
141.977622	60.452168	154.107688	42.344787	353.0	2010-03-05	par21	wisps
189.425514	11.906110	290.311290	74.440305	153.0	2012-05-19	par210	wisps
185.009109	29.367526	193.156600	82.732971	153.0	2012-05-20	par211	wisps
182.107285	45.675613	144.867719	69.577224	328.0	2012-05-20	par212	wisps
151.807263	36.592810	187.171260	54.162835	153.0	2012-06-19	par214	wisps
155.229117	34.569028	190.494123	57.047387	153.0	2012-06-19	par215	wisps
187.922063	-2.453822	293.017858	60.037214	356.0	2012-06-19	par216	wisps
190.271793	28.840226	175.490489	87.144876	253.0	2012-06-22	par217	wisps
216.795018	26.520583	36.790058	68.663659	153.0	2012-06-23	par218	wisps
175.452845	26.667108	210.658721	74.482016	253.0	2012-06-23	par219	wisps
133.185916	3.150745	224.790642	28.278717	253.0	2010-03-05	par22	wisps
172.954524	13.550355	245.113657	66.979146	153.0	2012-06-24	par220	wisps
217.426323	2.345275	350.635762	55.833085	253.0	2012-06-27	par221	wisps
212.546760	29.913710	46.727530	72.501595	303.0	2012-06-28	par222	wisps
186.974423	44.185176	136.925081	72.297879	406.0	2012-07-04	par224	wisps
186.968123	44.182205	136.942187	72.299357	178.0	2012-07-07	par226	wisps
186.974423	44.185176	136.925081	72.297879	406.0	2012-07-11	par227	wisps
187.674456	82.604340	123.740613	34.491319	381.0	2012-07-15	par228	wisps
21.060814	-58.735421	294.927812	-57.880123	306.0	2012-07-18	par229	wisps
145.815498	5.458513	230.069367	40.323002	684.0	2010-03-06	par23	wisps
16.316349	2.243826	129.946850	-60.439450	278.0	2012-07-19	par231	wisps

Table 6 *(continued)*

ra (deg)	dec(deg)	l (deg)	b (deg)	Exposure (s)	Observation Date (UT)	Pointing	Survey
14.743243	-36.039513	293.207422	-80.946019	406.0	2012-07-20	par232	wisps
185.199114	45.738679	139.048735	70.418716	153.0	2012-07-28	par233	wisps
341.470119	-46.854536	345.842192	-58.456435	353.0	2012-07-28	par234	wisps
228.065968	1.448846	1.665865	47.602767	406.0	2012-07-30	par235	wisps
231.203596	0.417886	3.422098	44.533308	406.0	2012-08-01	par236	wisps
192.618222	39.791933	123.777428	77.334735	303.0	2012-08-01	par237	wisps
192.850881	46.549351	122.949706	70.578900	406.0	2012-08-04	par238	wisps
258.742768	4.927988	26.086008	23.670269	253.0	2012-08-04	par239	wisps
184.672436	29.882628	190.060632	82.298758	278.0	2010-03-21	par24	wisps
241.244132	14.774671	27.726755	43.456687	406.0	2012-08-05	par240	wisps
72.538781	6.919767	191.536471	-23.022445	253.0	2012-08-08	par241	wisps
28.661021	4.888042	150.805806	-54.526855	356.0	2012-08-13	par242	wisps
207.031998	24.871345	26.055458	77.070977	253.0	2012-08-24	par243	wisps
3.829498	-79.930529	304.902571	-37.059131	303.0	2012-09-09	par244	wisps
147.436505	54.727624	160.138089	47.137443	153.0	2012-09-13	par245	wisps
149.815844	55.819404	157.863172	47.956608	328.0	2012-09-14	par246	wisps
12.130179	-12.802963	120.059739	-75.658439	203.0	2012-09-17	par247	wisps
310.121241	-6.744692	39.580321	-27.283694	406.0	2012-09-22	par248	wisps
5.940917	-74.296737	305.474328	-42.694631	153.0	2012-09-23	par249	wisps
152.174914	7.184972	232.645222	46.603662	734.0	2010-03-29	par25	wisps
129.830170	64.934188	150.652608	35.735620	203.0	2012-09-25	par250	wisps
66.569823	5.107070	189.494844	-28.951793	153.0	2012-10-01	par251	wisps
66.536063	5.072016	189.505683	-28.999434	153.0	2012-10-01	par252	wisps
168.457400	29.509161	200.845222	68.426460	1015.0	2012-10-16	par256	wisps
41.654328	-30.534856	227.521262	-64.614958	1818.0	2012-10-17	par257	wisps
38.238873	-37.367317	244.916656	-66.321032	406.0	2012-11-02	par258	wisps
175.659926	30.274343	197.084360	74.605523	278.0	2012-11-06	par259	wisps

Table 6 *(continued)*

ra (deg)	dec(deg)	l (deg)	b (deg)	Exposure (s)	Observation Date (UT)	Pointing	Survey
131.322285	22.915069	202.686150	34.626837	840.0	2010-04-01	par26	wisps
1.398618	-50.206967	320.659564	-65.313911	1365.0	2012-11-07	par260	wisps
2.944992	-6.884479	96.190220	-67.673413	1215.0	2012-11-09	par261	wisps
165.074783	12.228151	237.237689	60.007742	406.0	2012-11-11	par262	wisps
326.050164	14.811360	69.832602	-28.185447	128.0	2012-11-12	par263	wisps
165.289334	10.802163	239.791172	59.362143	253.0	2012-11-15	par264	wisps
144.113799	32.163859	193.922882	47.691728	406.0	2012-11-21	par267	wisps
111.018959	33.393336	185.128739	20.880987	203.0	2012-11-22	par268	wisps
40.181017	-8.248030	181.902550	-57.988447	153.0	2012-11-29	par269	wisps
173.272488	3.467523	261.187074	59.829280	1040.0	2010-04-02	par27	wisps
191.184904	2.288042	298.953994	65.108041	809.0	2012-12-01	par270	wisps
137.900424	18.535785	210.372657	39.009193	809.0	2012-12-02	par271	wisps
40.182042	-8.242677	181.895988	-57.984253	356.0	2012-12-06	par272	wisps
35.148273	0.595173	164.268812	-54.955934	356.0	2012-12-15	par273	wisps
29.926862	13.681390	147.148560	-45.955688	406.0	2012-12-18	par275	wisps
150.781770	32.759420	193.666995	53.345973	406.0	2013-01-08	par277	wisps
215.791801	0.032724	345.823018	55.075667	406.0	2013-01-25	par279	wisps
143.940243	14.462767	218.244060	42.857715	634.0	2010-04-02	par28	wisps
43.740797	-8.396277	186.068806	-55.306837	178.0	2013-01-27	par281	wisps
144.612114	7.167109	227.345412	40.159436	1015.0	2013-02-22	par288	wisps
191.099072	17.429987	293.050290	80.166365	406.0	2013-02-25	par289	wisps
180.744696	48.090088	143.966975	67.010932	328.0	2010-04-09	par29	wisps
236.301095	11.916848	21.163457	46.587833	278.0	2013-02-25	par290	wisps
217.911049	24.786255	32.645755	67.391573	153.0	2013-03-08	par292	wisps
146.158683	-19.689168	253.866303	24.900715	203.0	2013-03-11	par293	wisps
194.454312	-33.216045	304.466987	29.636688	1015.0	2013-03-16	par294	wisps
187.214099	10.760304	283.866667	72.790835	1015.0	2013-03-23	par295	wisps

Table 6 *(continued)*

ra (deg)	dec(deg)	l (deg)	b (deg)	Exposure (s)	Observation Date (UT)	Pointing	Survey
174.257634	1.782248	264.670408	59.011091	1015.0	2013-04-11	par297	wisps
138.666917	47.912584	171.387427	43.424786	2301.0	2013-05-03	par299	wisps
157.075694	39.286824	181.440775	57.944675	253.0	2010-04-21	par30	wisps
132.614738	44.804602	175.787610	39.399113	1262.0	2013-05-12	par300	wisps
215.192281	25.687672	33.882528	69.972017	153.0	2013-05-19	par301	wisps
41.226999	-30.034274	226.346269	-64.984385	1412.0	2013-05-28	par302	wisps
207.124195	26.555084	33.600596	77.266118	1315.0	2013-06-02	par303	wisps
217.216559	52.667143	94.173671	58.677326	2707.0	2013-05-29	par304	wisps
16.310264	2.263449	129.930283	-60.420603	1015.0	2013-06-15	par306	wisps
359.842649	-30.552302	13.136270	-78.103255	1215.0	2013-06-15	par307	wisps
239.129678	21.133239	35.214952	47.581265	1015.0	2013-06-21	par308	wisps
324.797994	-38.419686	4.595137	-48.536389	1015.0	2013-06-25	par309	wisps
130.864239	26.276506	198.616689	35.209914	659.0	2010-04-21	par31	wisps
240.815920	57.497578	88.701318	44.815451	1468.0	2013-07-20	par311	wisps
41.770151	-30.054275	226.402561	-64.514400	1165.0	2013-08-09	par312	wisps
42.149726	-30.558610	227.569943	-64.188171	1315.0	2013-08-06	par313	wisps
212.583702	23.021119	24.327858	71.690426	2901.0	2013-08-14	par314	wisps
350.715744	-70.480460	313.164058	-44.846824	1218.0	2013-08-20	par315	wisps
24.323292	-9.148688	156.145932	-69.009150	1015.0	2013-09-13	par317	wisps
133.499232	43.866890	177.020557	40.015418	1621.0	2013-10-30	par319	wisps
196.334411	-25.636778	306.862013	37.128879	484.0	2010-05-13	par32	wisps
116.381376	19.871518	200.459749	20.530027	2782.0	2013-12-06	par320	wisps
82.970192	-7.388645	210.513372	-21.032796	2154.0	2013-11-26	par321	wisps
130.581364	14.151459	212.136837	30.858700	1115.0	2013-12-09	par322	wisps
42.419466	27.315561	152.879295	-28.592506	2204.0	2013-12-18	par324	wisps
192.671339	-23.531902	302.708894	39.339519	2023.0	2013-12-21	par325	wisps
82.510557	-7.389325	210.297430	-21.441769	2126.0	2014-02-17	par326	wisps

Table 6 *(continued)*

ra (deg)	dec(deg)	l (deg)	b (deg)	Exposure (s)	Observation Date (UT)	Pointing	Survey
156.177048	48.183454	166.448631	54.658379	1265.0	2014-03-13	par328	wisps
151.430947	37.102862	186.336982	53.830665	1215.0	2014-03-17	par330	wisps
305.516555	-31.209644	11.429895	-31.971533	1165.0	2014-04-02	par332	wisps
152.055563	12.047684	226.293004	48.939300	2866.0	2014-04-05	par333	wisps
236.931515	20.962749	34.032454	49.485154	2326.0	2014-04-04	par335	wisps
151.325840	-24.360860	261.236363	24.759736	1165.0	2014-04-13	par336	wisps
165.567626	5.320233	248.039506	56.077105	1115.0	2014-04-14	par337	wisps
178.729387	19.669545	239.870725	75.056898	1215.0	2014-04-15	par338	wisps
143.739721	2.033297	232.370878	36.747612	709.0	2010-05-19	par34	wisps
194.126300	32.468353	111.609983	84.548079	1721.0	2014-05-01	par340	wisps
151.643558	23.627469	208.909926	52.760085	1215.0	2014-03-20	par341	wisps
322.946349	-12.040380	40.658412	-40.966462	1318.0	2014-04-06	par342	wisps
151.925274	10.069809	228.815351	47.878408	1112.0	2014-05-15	par343	wisps
214.863780	6.114224	351.781481	60.346219	1421.0	2014-05-29	par345	wisps
216.765770	23.886918	29.723069	68.215698	1165.0	2014-05-31	par346	wisps
155.833539	4.145259	239.378912	47.870939	1771.0	2014-06-02	par347	wisps
195.264650	27.839901	51.929167	87.750785	1165.0	2014-06-04	par348	wisps
151.386332	-23.085826	260.363342	25.762452	962.0	2014-06-05	par349	wisps
195.942651	29.883973	79.144064	86.135843	634.0	2010-05-21	par35	wisps
208.307823	36.324577	71.819743	73.995606	1365.0	2014-06-14	par350	wisps
172.230693	-4.424342	267.524153	52.680439	1671.0	2014-06-01	par352	wisps
212.060758	56.945278	103.590490	57.204856	506.0	2014-06-28	par353	wisps
343.544634	16.223489	86.219081	-38.149959	1268.0	2014-05-10	par354	wisps
351.256344	-40.605975	350.292779	-67.668090	1265.0	2014-07-07	par355	wisps
356.276282	-42.659761	339.619038	-69.432791	1518.0	2014-07-10	par356	wisps
188.062187	6.023171	289.870505	68.406932	1771.0	2014-05-31	par357	wisps
357.754947	-43.391869	335.939047	-69.658950	2782.0	2014-07-08	par358	wisps

Table 6 continued on next page

Table 6 *(continued)*

ra (deg)	dec(deg)	l (deg)	b (deg)	Exposure (s)	Observation Date (UT)	Pointing	Survey
353.819704	-35.604662	0.630685	-71.711732	1290.0	2014-07-13	par359	wisps
205.128070	41.386073	90.826581	72.544030	1612.0	2010-05-27	par36	wisps
216.482339	0.654232	347.443114	55.141197	1721.0	2014-07-30	par360	wisps
208.564791	18.043379	4.094929	72.913697	1165.0	2014-07-31	par361	wisps
196.047035	31.152826	89.021694	85.106967	1115.0	2014-08-09	par362	wisps
57.939376	-14.424475	205.444506	-46.237681	1318.0	2014-08-15	par364	wisps
21.403878	-0.013796	141.176695	-61.668898	4278.0	2014-07-04	par365	wisps
226.410501	3.654840	2.616019	50.288310	1265.0	2014-08-29	par367	wisps
350.641997	-34.845296	5.356401	-69.506860	1696.0	2014-08-29	par368	wisps
324.412205	-14.636785	38.277579	-43.345950	2276.0	2014-08-27	par369	wisps
205.128070	41.386073	90.826581	72.544030	1237.0	2010-05-30	par37	wisps
243.753484	-9.656187	3.431116	28.484961	1165.0	2014-09-03	par370	wisps
301.437186	-41.666336	358.626464	-30.993985	1218.0	2014-09-06	par371	wisps
342.188884	-80.177751	309.063490	-35.442573	2304.0	2014-08-25	par372	wisps
351.289384	-12.203886	65.137550	-64.870186	3338.0	2014-10-26	par374	wisps
154.088076	-27.764916	265.699856	23.676560	1165.0	2014-11-23	par375	wisps
255.387751	64.132500	94.300021	36.115933	1265.0	2014-12-01	par377	wisps
217.354067	32.411824	52.835599	68.145254	1115.0	2014-12-08	par378	wisps
186.303170	-2.819621	289.989286	59.391508	709.0	2010-05-31	par38	wisps
162.010906	15.262185	229.096687	58.999301	1215.0	2014-12-21	par380	wisps
59.417632	-13.499878	205.099561	-44.548248	1365.0	2015-01-05	par381	wisps
264.840162	45.920256	72.219223	31.270944	2204.0	2015-01-12	par382	wisps
217.871228	24.796485	32.653285	67.429032	1165.0	2015-03-29	par385	wisps
221.513304	3.907210	357.644788	54.120331	1165.0	2015-06-14	par386	wisps
139.453306	27.383551	199.673887	42.908797	1190.0	2015-11-30	par387	wisps
161.884433	13.091660	232.603292	57.835156	1112.0	2015-12-01	par388	wisps
184.606947	29.168764	195.344098	82.444861	1162.0	2015-12-05	par389	wisps

Table 6 *(continued)*

ra (deg)	dec(deg)	l (deg)	b (deg)	Exposure (s)	Observation Date (UT)	Pointing	Survey
152.406815	30.012332	198.488491	54.538149	328.0	2010-06-04	par39	wisps
225.095349	41.465472	69.848999	60.003517	1848.0	2015-12-17	par391	wisps
233.687179	50.247364	80.887050	51.371555	809.0	2015-12-24	par394	wisps
192.104350	17.695183	298.550216	80.541222	834.0	2016-01-08	par395	wisps
5.844536	15.709914	113.075255	-46.624117	431.0	2016-01-17	par396	wisps
187.892932	12.082625	284.760332	74.249297	784.0	2016-01-24	par397	wisps
260.040721	48.096424	74.413146	34.742928	2371.0	2016-02-08	par398	wisps
34.083395	-39.038725	252.263581	-68.683127	584.0	2010-06-04	par40	wisps
27.200360	18.956035	141.265914	-41.864457	1268.0	2016-02-15	par400	wisps
152.775378	-4.760968	246.233569	39.846599	1396.0	2016-03-06	par402	wisps
198.718013	26.196139	24.161214	84.682643	431.0	2016-03-08	par403	wisps
336.427433	-72.217068	316.786153	-40.759642	1418.0	2016-03-09	par404	wisps
184.658681	29.309224	194.223458	82.454023	884.0	2016-03-10	par405	wisps
152.757775	-4.793049	246.249546	39.812155	940.0	2016-03-13	par406	wisps
152.754996	-4.801030	246.254900	39.804776	456.0	2016-03-15	par407	wisps
152.671578	-4.761982	246.145003	39.768674	706.0	2016-03-18	par408	wisps
231.262938	4.387884	7.979306	46.910434	909.0	2016-03-19	par409	wisps
182.114689	45.645851	144.895295	69.605861	1084.0	2010-06-14	par41	wisps
185.403785	4.598705	284.103282	66.374131	784.0	2016-03-21	par411	wisps
213.830725	4.835323	348.530981	60.055998	431.0	2016-03-22	par412	wisps
171.071089	11.527996	246.022911	64.271890	784.0	2016-03-23	par413	wisps
171.893254	11.914622	246.562274	65.134694	1115.0	2016-03-30	par416	wisps
137.052967	32.767090	191.988344	41.864139	506.0	2016-03-30	par417	wisps
178.714604	57.705058	137.129392	57.836373	656.0	2016-04-09	par420	wisps
186.107122	61.198085	128.690435	55.627160	909.0	2016-04-13	par422	wisps
190.443997	32.277825	144.510060	84.439955	1293.0	2016-04-19	par425	wisps
147.226228	13.828262	220.877596	45.501731	5857.0	2016-04-30	par427	wisps

Table 6 *(continued)*

ra (deg)	dec(deg)	l (deg)	b (deg)	Exposure (s)	Observation Date (UT)	Pointing	Survey
217.995819	9.977284	1.832227	60.753217	431.0	2016-05-05	par428	wisps
316.032667	-7.381284	42.041188	-32.787289	909.0	2010-06-16	par43	wisps
183.352089	-13.671511	289.007202	48.169366	2557.0	2016-05-12	par430	wisps
137.623300	33.459227	191.157189	42.436462	531.0	2016-05-11	par431	wisps
205.923415	18.733734	0.730132	75.346265	278.0	2016-05-15	par432	wisps
205.229161	28.408877	42.470060	78.985200	1268.0	2016-06-25	par433	wisps
176.097856	7.218626	261.249714	64.517617	909.0	2016-05-20	par434	wisps
224.196007	53.412019	90.210834	55.007688	809.0	2016-05-25	par435	wisps
201.377941	22.554692	4.168014	81.022079	581.0	2016-05-26	par436	wisps
179.277329	32.318763	185.903527	77.126887	934.0	2016-06-03	par437	wisps
151.190534	52.987143	161.295962	49.846624	809.0	2016-06-06	par438	wisps
190.671891	35.631028	134.761446	81.295316	1240.0	2016-06-09	par439	wisps
168.060621	35.614210	184.873370	67.269590	709.0	2010-06-17	par44	wisps
172.347110	60.399813	140.024105	53.921150	984.0	2016-06-09	par440	wisps
192.051540	17.861265	298.166487	80.703096	1746.0	2016-06-18	par441	wisps
149.793324	50.674645	165.125285	49.886921	809.0	2016-06-23	par442	wisps
203.814219	8.028896	333.468906	68.263036	759.0	2016-06-29	par443	wisps
207.745546	27.868547	39.574760	76.783081	884.0	2016-06-30	par444	wisps
237.940534	20.098762	33.230883	48.318214	1268.0	2016-07-01	par445	wisps
234.989964	-2.087768	4.012478	40.014562	1923.0	2016-07-03	par446	wisps
254.767645	37.596767	61.008617	37.607258	381.0	2016-07-07	par447	wisps
235.746988	-10.847548	356.375038	33.684553	1240.0	2016-07-09	par449	wisps
189.361149	1.421725	294.911319	64.075340	797.0	2010-06-20	par45	wisps
211.516532	25.122834	30.303000	73.145327	1218.0	2016-07-10	par450	wisps
182.233770	26.224752	215.961435	80.465358	934.0	2016-07-16	par451	wisps
227.281719	37.503432	61.426622	59.318534	481.0	2016-07-18	par452	wisps
243.453767	26.504622	44.229401	45.160407	1746.0	2016-07-22	par453	wisps

Table 6 *(continued)*

ra (deg)	dec(deg)	l (deg)	b (deg)	Exposure (s)	Observation Date (UT)	Pointing	Survey
53.349150	-40.958823	246.184361	-54.101200	3185.0	2016-07-28	par454	wisps
229.812484	28.592049	44.283573	57.426575	1593.0	2016-08-10	par456	wisps
233.727694	12.870834	20.732303	49.260621	506.0	2016-08-11	par457	wisps
210.659503	54.168901	101.981593	59.967735	706.0	2016-08-13	par458	wisps
229.990269	25.509293	38.715679	56.798931	1268.0	2016-09-06	par459	wisps
339.494767	-18.699296	41.167450	-58.239881	328.0	2010-06-20	par46	wisps
75.280824	-5.806904	205.184185	-27.132799	481.0	2016-09-16	par461	wisps
50.557507	-17.931791	206.143563	-54.133199	1468.0	2016-09-23	par462	wisps
69.483414	-11.105133	207.720922	-34.629680	431.0	2016-09-22	par463	wisps
75.548958	-7.011412	206.526227	-27.448092	431.0	2016-09-22	par464	wisps
48.913738	-21.676600	211.482065	-56.831301	581.0	2016-09-23	par465	wisps
49.583414	-16.871926	203.852257	-54.585855	656.0	2016-09-24	par466	wisps
51.505596	-16.728430	204.853488	-52.837793	303.0	2016-09-25	par467	wisps
168.815971	52.933213	151.071782	58.620582	1040.0	2016-09-28	par468	wisps
129.368643	44.459439	176.116167	37.077898	631.0	2016-09-29	par469	wisps
199.882375	27.443706	37.433024	83.751413	587.0	2010-06-25	par47	wisps
164.996391	40.644716	175.256466	63.382103	909.0	2016-10-04	par471	wisps
137.759674	33.515920	191.101889	42.556826	934.0	2016-10-05	par472	wisps
343.401926	-6.751855	63.603606	-55.402995	481.0	2016-10-11	par473	wisps
175.283957	11.629721	252.725555	67.360540	784.0	2016-11-03	par474	wisps
210.118388	57.403588	105.696802	57.354548	328.0	2016-11-21	par476	wisps
171.338899	53.345583	148.353599	59.326114	253.0	2016-12-06	par477	wisps
146.763759	51.434897	164.936824	47.840405	1468.0	2016-12-08	par478	wisps
80.182331	-25.420267	227.929004	-30.373670	1671.0	2016-12-19	par480	wisps
176.741087	-14.196039	280.217042	45.812877	1143.0	2016-12-22	par481	wisps
49.793782	-32.833102	232.178833	-57.669717	1726.0	2017-01-01	par482	wisps
41.713122	-1.083452	174.527483	-51.997455	1418.0	2017-01-05	par483	wisps

Table 6 *(continued)*

ra (deg)	dec(deg)	l (deg)	b (deg)	Exposure (s)	Observation Date (UT)	Pointing	Survey
221.183917	34.462369	56.747793	64.684275	1093.0	2010-07-02	par49	wisps
216.782252	57.859823	100.854007	54.974494	1034.0	2009-12-20	par5	wisps
335.584799	9.612644	73.229724	-38.470633	328.0	2010-07-08	par50	wisps
228.304474	36.555337	59.374302	58.649675	278.0	2010-07-10	par51	wisps
202.591790	28.182489	42.150579	81.317768	634.0	2010-07-16	par52	wisps
227.800767	40.426747	66.797789	58.327150	253.0	2010-07-17	par53	wisps
236.234908	48.756031	77.799636	50.294775	303.0	2010-07-18	par54	wisps
185.225541	-2.080361	287.592105	59.878822	909.0	2010-07-22	par55	wisps
244.208476	6.611212	19.838310	37.204818	684.0	2010-07-28	par56	wisps
188.317827	47.888905	131.428719	68.938527	203.0	2010-07-31	par57	wisps
188.179627	-0.560930	292.941831	61.947180	609.0	2010-08-01	par58	wisps
237.591319	39.987509	63.910618	51.027566	734.0	2010-08-04	par59	wisps
27.570390	13.068069	144.342855	-47.342606	609.0	2009-12-24	par6	wisps
219.368886	-1.831670	348.570577	51.392063	1112.0	2010-08-18	par64	wisps
244.720069	33.665338	54.517065	45.253389	1243.0	2010-08-19	par65	wisps
219.369679	-1.833079	348.570119	51.390472	1237.0	2010-08-22	par66	wisps
353.384530	39.355464	106.893933	-21.077971	1215.0	2010-10-14	par68	wisps
231.030449	9.913295	14.752941	50.151058	1087.0	2010-09-12	par69	wisps
228.519783	36.283905	58.817296	58.510467	909.0	2011-08-04	par71	wisps
238.712085	36.397703	58.187559	50.311616	909.0	2010-09-21	par72	wisps
211.304475	46.986493	91.681148	65.415224	1034.0	2010-09-30	par73	wisps
137.702566	10.290439	219.805422	35.574062	1065.0	2010-10-02	par74	wisps
138.929303	47.967898	171.284135	43.593142	406.0	2010-10-06	par75	wisps
201.844487	44.508984	102.731950	71.182849	887.0	2010-10-07	par76	wisps
356.254109	15.165467	100.082341	-44.739230	381.0	2010-10-13	par77	wisps
17.536926	-2.423583	134.002001	-64.892427	1187.0	2010-11-08	par79	wisps
17.538117	-2.373982	133.984802	-64.843352	1187.0	2010-11-18	par80	wisps

Table 6 *(continued)*

ra (deg)	dec(deg)	l (deg)	b (deg)	Exposure (s)	Observation Date (UT)	Pointing	Survey
17.537465	-2.373823	133.983230	-64.843306	1187.0	2010-11-19	par81	wisps
242.208745	60.236371	91.863029	43.129263	481.0	2010-11-21	par82	wisps
17.544100	-2.405082	134.011182	-64.872972	859.0	2010-11-23	par83	wisps
17.531141	-2.422277	133.988054	-64.892128	1162.0	2010-11-24	par84	wisps
134.665658	29.148501	196.166375	39.180225	353.0	2010-11-28	par85	wisps
168.896576	42.860198	167.717626	65.000519	759.0	2010-11-29	par86	wisps
146.696040	47.251098	171.040610	48.873153	912.0	2010-12-03	par87	wisps
147.746625	11.764222	223.832708	45.060351	559.0	2010-12-04	par88	wisps
17.541075	-2.374644	133.991918	-64.843499	1187.0	2010-12-07	par89	wisps
15.234184	2.431665	127.732359	-60.351517	772.0	2010-12-10	par90	wisps
17.523379	-2.419903	133.969091	-64.891112	909.0	2010-12-10	par91	wisps
141.533093	12.648313	219.160899	39.977555	278.0	2010-12-10	par92	wisps
184.664811	29.738487	191.099288	82.338080	278.0	2010-12-23	par93	wisps
331.360425	-0.299171	59.880696	-41.985555	1623.0	2010-12-13	par94	wisps
17.517345	-2.417532	133.954141	-64.889803	909.0	2011-01-02	par95	wisps
32.351026	-4.730598	166.060988	-60.895121	4294.0	2010-12-16	par96	wisps
17.525232	-2.397958	133.964576	-64.869172	859.0	2011-01-16	par97	wisps
151.922157	50.223162	165.053464	51.314909	353.0	2011-01-22	par98	wisps
144.243053	29.530798	197.812946	47.449732	634.0	2011-01-28	par99	wisps

REFERENCES

Allers, K., Jaffe, D., Luhman, K., et al. 2007, \apj, 657, 511

Atek, H., Malkan, M., McCarthy, P., et al. 2010, \apj, 723, 104

Aumer, M., & Binney, J. 2009, \mnras, 397, 1286

Baraffe, I., Chabrier, G., Allard, F., & Hauschildt, P. 2003, in IAU Symposium, Vol. 211, Brown Dwarfs, ed. E. Martín, 41–+

Bardalez Gagliuffi, D., Burgasser, A., Gelino, C., et al. 2014, \apj, 794, 143

Bardalez Gagliuffi, D. C., Burgasser, A. J., Schmidt, S. J., et al. 2019, arXiv e-prints, arXiv:1906.04166

Basri, G. 1998, in Astronomical Society of the Pacific Conference Series, Vol. 134, Brown Dwarfs and Extrasolar Planets, ed. R. Rebolo, E. Martin, & M. Zapatero Osorio, 394–+

Bastian, N., Covey, K., & Meyer, M. 2010, \araa, 48, 339

Bochanski, J., Hawley, S., Covey, K., et al. 2010, \aj, 139, 2679

Brammer, G., van Dokkum, P., Franx, M., et al. 2012, \apjs, 200, 13

Burgasser, A. 2001, PhD thesis, AA(Department of Physics, California Institute of Technology)

—. 2004, \apjs, 155, 191

—. 2007, \apj, 659, 655

—. 2014a, ArXiv e-prints, arXiv:1406.4887

Burgasser, A., Geballe, T., Leggett, S., Kirkpatrick, J., & Golimowski, D. 2006, \apj, 637, 1067

Burgasser, A., Looper, D., Kirkpatrick, J., & Liu, M. 2007, \apj, 658, 557

Burgasser, A., Witte, S., Helling, C., et al. 2009, \apj, 697, 148

Burgasser, A. J. 2014b, arXiv:1406.4887

Burningham, B., Cardoso, C., Smith, L., et al. 2013, \mnras, 433, 457

Burrows, A., Hubbard, W., Lunine, J., & Liebert, J. 2001, Reviews of Modern Physics, 73, 719

Carnero Rosell, A., Santiago, B., dal Ponte, M., et al. 2019, arXiv e-prints, arXiv:1903.10806

Chabrier, G. 2001, \apj, 554, 1274

Chabrier, G., & Baraffe, I. 2000, \araa, 38, 337

Chabrier, G., & Mera, D. 1997, A&A, 328, 83

Collaboration, T. A., Robitaille, T. P., Tollerud, E. J., et al. 2013, arXiv:1307.6212

Cruz, K., Reid, I., Kirkpatrick, J., et al. 2007, \aj, 133, 439

Cushing, M., Tokunaga, A., & Kobayashi, N. 2000, \aj, 119, 3019

Cushing, M., Kirkpatrick, J., Gelino, C., et al. 2011, \apj, 743, 50

Davis, M., Guhathakurta, P., Konidaris, N. P., et al. 2007, The Astrophysical Journal Letters, 660, L1

Day-Jones, A., Marocco, F., Pinfield, D., et al. 2013, \mnras, 430, 1171

Delfosse, X., Tinney, C. G., Forveille, T., et al. 1999, Astron. Astrophys. Suppl. Ser., 135, 41

Dupuy, T., & Liu, M. 2012, \apjs, 201, 19

Faherty, J. K., Bochanski, J. J., Gagne, J., et al. 2018, The Astrophysical Journal, 863, 91

Filippazzo, J. C., Rice, E. L., Faherty, J., et al. 2015, Astrophysical Journal, 810, 158

Gagné, J., Faherty, J. K., Cruz, K. L., et al. 2015, arXiv:1506.07712

Giavalisco, M., Ferguson, H. C., Koekemoer, A. M., et al. 2004, The Astrophysical Journal, 600, L93

Gould, A., Bahcall, J., & Flynn, C. 1997, \apj, 482, 913

Hardegree-Ullman, K. K., Cushing, M. C., Muirhead, P. S., & Christiansen, J. L. 2019, arXiv e-prints, arXiv:1905.05900

Holwerda, B. W., Trenti, M., Clarkson, W., et al. 2014, The Astrophysical Journal, 788, 77

Jones, E., Oliphant, T., Peterson, P., et al. 2001–, SciPy: Open source scientific tools for Python, , , [Online; accessed ¡today¿]

Jurić, M., Ivezić, Ž., Brooks, A., et al. 2008, \apj, 673, 864

Kerins, E. J. 1997, A&A, 328, 5

Kimble, R. A., MacKenty, J. W., O'Connell, R. W., & Townsend, J. A. 2008, Wide Field Camera 3: a powerful new imager for the Hubble Space Telescope, , , doi:10.1117/12.789581

Kirkpatrick, J. 2005, \araa, 43, 195

Kirkpatrick, J., Looper, D., Burgasser, A., et al. 2010, \apjs, 190, 100

Kirkpatrick, J., Cushing, M., Gelino, C., et al. 2011, \apjs, 197, 19

Kirkpatrick, J. D., Reid, I. N., Liebert, J., et al. 2000, The Astronomical Journal, 120, 447

Kirkpatrick, J. D., Martin, E. C., Smart, R. L., et al. 2019, ApJS, 240, 19

Kümmel, M., Walsh, J. R., Pirzkal, N., Kuntschner, H., & Pasquali, A. 2009, Publications of the Astronomical Society of the Pacific, 121, 59

Kuntschner, H., Kümmel, M., & Walsh, J. R. 2013

Lawrence, A., & Others. 2007, \mnras, 379, 1599

Lodieu, N., Espinoza Contreras, M., Zapatero Osorio, M. R., et al. 2017, Astronomy & Astrophysics, 598, A92

Lopez-Santiago, J., Montes, D., Crespo-Chacon, I., & Fernandez-Figueroa, M. J. 2006, The Astrophysical Journal, 643, 1160

LSST Science Collaboration, L. S., Abell, P. A., Allison, J., et al. 2009, arXiv:0912.0201

Luhman, K. L., & Mamajek, E. E. 2012, The Astrophysical Journal, 758, 31

Mamajek, E. E. 2015, Proceedings of the International Astronomical Union, 10, 21

Manjavacas, E., Apai, D., Zhou, Y., et al. 2018, arXiv:1812.03963

Marocco, F., Jones, H. R. A., Day-Jones, A. C., et al. 2015, Monthly Notices of the Royal Astronomical Society, 449, 3651

Martin, E. C., Mace, G. N., McLean, I. S., et al. 2017, The Astrophysical Journal, 838, 73

Masters, D., McCarthy, P., Burgasser, A., et al. 2012, \apjl, 752, L14

Metchev, S., Kirkpatrick, J., Berriman, G., & Looper, D. 2008, \apj, 676, 1281

Momcheva, I. G., Brammer, G. B., van Dokkum, P. G., et al. 2016, The Astrophysical Journal Supplement Series, 225, 27

Pedregosa, F., Varoquaux, G., Gramfort, A., et al. 2012, arXiv e-prints, arXiv:1201.0490

Pirzkal, N., Sahu, K., Burgasser, A., et al. 2005, \apj, 622, 319

Pirzkal, N., Burgasser, A., Malhotra, S., et al. 2009, \apj, 695, 1591

Reid, I., Kirkpatrick, J., Liebert, J., et al. 1999, \apj, 521, 613

Reylé, C. 2018, Astronomy & Astrophysics, 619, L8

Reylé, C., & Robin, A. C. 2001, A&A, 373, 886

Reyle, C., Delorme, P., Willott, C. J., et al. 2010, Astronomy and Astrophysics, Volume 522, id.A112, 15 pp., 522, arXiv:1008.2301

Rujopakarn, W., Eisenstein, D. J., Rieke, G. H., et al. 2010, ApJ, 718, 1171

Ryan, R. E., Thorman, P. A., Yan, H., et al. 2011, The Astrophysical Journal, 739, 83

Ryan, R. E., Thorman, P. A., Schmidt, S. J., et al. 2017, The Astrophysical Journal, 847, 53

Ryan Jr., R., Hathi, N., Cohen, S., & Windhorst, R. 2005, \apjl, 631, L159

Ryan Jr., R. E., & Reid, I. N. 2016, The Astronomical Journal, 151, 92

Schneider, A. C., Cushing, M. C., Kirkpatrick, J. D., et al. 2015, The Astrophysical Journal, 804, 92

Scoville, N., Aussel, H., Brusa, M., et al. 2007, The Astrophysical Journal Supplement Series, 172, 1

Skelton, R. E., Whitaker, K. E., Momcheva, I. G., et al. 2014, The Astrophysical Journal Supplement Series, 214, 24

Sorahana, S., Nakajima, T., & Matsuoka, Y. 2018, arXiv:1811.07496

Spergel, D., Gehrels, N., Baltay, C., et al. 2015, arXiv:1503.03757

Tokunaga, A., & Kobayashi, N. 1999, \aj, 117, 1010

Van Vledder, I., Van Der Vlugt, D., Holwerda, B. W., et al. 2016, Monthly Notices of the Royal Astronomical Society, 458, 425

Zhang, Z. H., Burgasser, A. J., Gálvez-Ortiz, M. C., et al. 2019, MNRAS, 486, 1260